Mast cells acquire MHCII from dendritic cells during skin inflammation

Jan Dudeck,[1,2]* Anna Medyukhina,[4]* Julia Fröbel,[1] Carl-Magnus Svensson,[4] Johanna Kotrba,[1] Michael Gerlach,[3,5,6] Ann-Christine Gradtke,[7] Bernd Schröder,[7] Stephan Speier,[3,5,6] Marc Thilo Figge,[4,8]** and Anne Dudeck[1,2]**

[1]Institute for Molecular and Clinical Immunology, Medical Faculty, Otto-von-Guericke University Magdeburg, Magdeburg, Germany
[2]Institute for Immunology, Medical Faculty Carl-Gustav Carus and [3]DFG-Center for Regenerative Therapies Dresden, Faculty of Medicine, Technische Universität Dresden, Dresden, Germany
[4]Applied Systems Biology, Leibniz Institute for Natural Product Research and Infection Biology, Hans-Knöll-Institute, Jena, Germany
[5]Paul Langerhans Institute Dresden of Helmholtz Centre Munich at the University Clinic Carl Gustav Carus of the Technische Universität Dresden, Helmholtz Zentrum München, German Research Center for Environmental Health, Neuherberg, Germany
[6]German Centre for Diabetes Research, Dresden, Germany
[7]Institute of Biochemistry, Christian-Albrechts-Universität zu Kiel, Kiel, Germany
[8]Faculty of Biology and Pharmacy, Friedrich Schiller University Jena, Jena, Germany

Mast cells (MCs) and dendritic cells (DCs) are essential innate sentinels populating host-environment interfaces. Using longitudinal intravital multiphoton microscopy of DC^{GFP}/MC^{RFP} reporter mice, we herein provide in vivo evidence that migratory DCs execute targeted cell-to-cell interactions with stationary MCs before leaving the inflamed skin to draining lymph nodes. During initial stages of skin inflammation, DCs dynamically scan MCs, whereas at a later stage, long-lasting interactions predominate. These innate-to-innate synapse-like contacts ultimately culminate in DC-to-MC molecule transfers including major histocompatibility complex class II (MHCII) proteins enabling subsequent ex vivo priming of allogeneic T cells with a specific cytokine signature. The extent of MHCII transfer to MCs correlates with their T cell priming efficiency. Importantly, preventing the cross talk by preceding DC depletion decreases MC antigen presenting capacity and T cell–driven inflammation. Consequently, we identify an innate intercellular communication arming resident MCs with key DC functions that might contribute to the acute defense potential during critical periods of migration-based DC absence.

INTRODUCTION

Mast cells (MCs) and dendritic cells (DCs) represent innate sentinel cells populating host-environment interfaces including the skin to ensure host defense against invading pathogens or sterile damage. MCs are known as key mediators of type I allergic reactions, in the worst case culminating in life-threatening anaphylaxis (Galli and Tsai, 2012; Blank et al., 2013). In the last decade, various important MC functions in innate and adaptive immunity have been reported (Galli et al., 2005; Abraham and St. John, 2010; St. John and Abraham, 2013). For example, we have demonstrated that MCs critically promote neutrophil recruitment to sites of inflammation (Dudeck et al., 2011a; De Filippo et al., 2013; Weber et al., 2015). Moreover, we found MCs to be essential for efficient T cell expansion in contact hypersensitivity (CHS) responses or Freund's adjuvant-based vaccination, very likely because of the MC impact on DC migration and function (Dudeck et al., 2011a, 2015; Schubert et al., 2015). In CHS, contact allergens, so-called haptens, modify self-proteins and thereby render them immunogenic. DCs engulf haptenated proteins and migrate to skin-draining LNs to prime effector T cells that initiate a hapten-specific skin inflammation upon second hapten encounter (Kaplan et al., 2012; Martin, 2012, 2015). The primary effector cells of adaptive responses to dinitrofluorobenzene (DNFB) are IFN-γ–producing $CD8^+$ T cells, whereas $CD4^+$ T cells regulate the magnitude and duration of inflammation (Gocinski and Tigelaar, 1990; Gorbachev et al., 2001). The mechanisms underlying MC effects on DC activation and migration presumably include TNF and histamine but are still poorly defined (Jawdat et al., 2006; Suto et al., 2006; Shelburne et al., 2009; Otsuka et al., 2011). Our previous observation that in vitro DC/MC interaction enhances DC maturation (Dudeck et al., 2011b) led us to hypothesize that DCs may as well actively communicate with MCs in inflamed skin in vivo. However, so far an intercellular interaction between DCs and MCs has been reported only

*J. Dudeck and A. Medyukhina contributed equally to this paper.

**M.T. Figge and A. Dudeck contributed equally to this paper.

Correspondence to Anne Dudeck: anne.dudeck@med.ovgu.de; Marc Thilo Figge: thilo.figge@leibniz-hki.de

Abbreviations used: 2D, two-dimensional; 3D, three-dimensional; BM, bone marrow; BP, bandpass filter; CHS, contact hypersensitivity; CTMC, connective tissue–type MC; DC, dendritic cell; dDC, dermal DC; DNFB, dinitrofluorobenzene; DT, diphtheria toxin; i.d., intradermal; MC, mast cell; MIP, maximum intensity projection; ROI, region of interest; SHG, second harmonic generation.

The Rockefeller University Press
J. Exp. Med. 2017 Vol. 214 No. 12 3791–3811
https://doi.org/10.1084/jem.20160783

in vitro (Dudeck et al., 2011b; Otsuka et al., 2011), and a possible reverse impact of DCs on MC functionality has not been described so far. In this study, we examined MC and DC dynamics during the progress of skin inflammation in vivo by means of longitudinal intravital multiphoton microscopy of MC/DC double reporter mice. We further performed a comparative automated computational image analysis of DC and MC features before and after hapten encounter from randomly chosen images, enabling a robust quantitative evaluation. We have previously shown that image-based systems biology approaches (Figge and Meyer-Hermann, 2011; Medyukhina et al., 2015) are powerful tools to investigate dynamical, functional, and morphological aspects of complex biological systems—for example, applying intravital multiphoton–based microscopy to characterize lymphocyte migration in LNs (Figge et al., 2008; Meyer-Hermann et al., 2009; Coelho et al., 2013; Mokhtari et al., 2013) and affinity maturation of antibodies in germinal centers (Garin et al., 2010; Zhang et al., 2013). Here, we demonstrate that skin inflammation initiates an intensive and long-lasting DC-to-MC interaction that ultimately culminates in the functional transfer of DC-restricted proteins to MCs.

RESULTS

To study MC and DC co-occurrence and possible communication under physiological and inflammatory conditions in vivo, we generated DC/MC double reporter mice, hereafter referred to as DC^{GFP}/MC^{RFP}. We bred the DC reporter line CD11c-EGFP/DTR (Jung et al., 2002) with the MC-specific Mcpt5-Cre line (Scholten et al., 2008; Dudeck et al., 2011a) crossed to the excision reporter line R26_tdRFP (Luche et al., 2007). DC and MC dynamics were monitored longitudinally before and during contact allergen–induced skin inflammation by means of noninvasive, intravital multiphoton microscopy.

High-throughput image quantification

To characterize DC and MC responses to contact sensitizers in an objective manner, we used an automated high-throughput quantification of static z-stacks of images and time-lapse series. We developed a three-step automated image analysis procedure (Fig. 1), which included preprocessing of images, image segmentation, and quantitative analysis. The purpose of the preprocessing step (Fig. 1 B) was to enhance image quality in order to facilitate cell detection. Segmentation of image data (Fig. 1 C) included a specific procedure for artifacts removal to get rid of nonspecific autofluorescence from hairs and corneocytes, which usually occur in RFP and GFP channels simultaneously (Fig. 1 D). Hence, to distinguish between cells and artifacts (Fig. S1) in addition to RFP and GFP intensities, we examined the size and shape of objects, as well as corresponding second harmonic generation (SHG) signal, which represents the collagen content and is usually high in skin, except for the regions of corneocytes and hair follicles. After artifacts removal, touching cells were separated using the three-dimensional (3D) seeded watershed transformation, which enabled further quantitative characterization of individual MCs. The detection of individual MCs reached high sensitivity and precision values of 95% and 99%, respectively.

Phenotypic response of dermal DCs and MCs to hapten-induced skin inflammation

In healthy ear skin, dermal DCs (dDCs) were heterogeneously distributed over time with varying motilities and velocities. Monitoring the inflammation-induced dDC behavior by longitudinal intravital imaging, we surprisingly observed that all dDCs were paralyzed within the first 2 h after DNFB application for at least 6 to 7 h. Thereafter, dDCs gradually regained on-site motility followed by an increased migratory activity exceeding nonstimulated conditions (Fig. 2 and Video 1). Because hapten-induced MC activation (Dudeck et al., 2011a) may lead to this DC migrational arrest as a means of ensuring efficient antigen uptake and/or gene induction via prostaglandin D2 (PDG2) release that is known to elicit migratorial arrest of DCs, we tested whether hapten administration was followed by PDG2 release and if DC arrest was affected by blocking of PDG2 via injection of a DP-1 antagonist. However, neither were the PDG2 levels altered upon hapten-induced MC activation nor did the DP-1 antagonist alter the extent or kinetic of DC migrational arrest (not depicted), indicating its independence of PDG2 release. Based on the DC migrational behavior, we determined further imaging time frames at 10 ± 2 h and 26 ± 2 h after DNFB administration.

In contrast to dDCs, MCs were homogeneously distributed in the dermis with close proximity to blood vessels and hair follicles (Fig. 3). Within the first hours after DNFB administration, MCs responded with a profound contraction from an elongated and in some cases even spindle-like morphology to a globular cell shape that remained for at least 48 h. The computational analysis proved a significant reduction in MC eccentricity at 10 ± 2 h and 26 ± 2 h after DNFB administration as compared with the cell shapes before DNFB treatment, whereas the cell volume was not markedly altered (Fig. 3, B and C). Importantly, MCs remained completely stationary in the skin tissue without noteworthy MC migration in response to skin inflammation. Computational analysis of cell shape dynamics using time lapse series showed a decrease of changes in the MC shape over time at later time points of DNFB treatment, which even demonstrates a reduced MC in place motility (Fig. 3, D and E).

Inflammation-induced dynamic DC-to-MC communication

Directly after remobilization, ~8 h after DNFB, dDCs started to frequently contact the stationary MCs and initiated intensive cell-to-cell interactions (Fig. 4, A and B; and Videos 2, 3, and 4). Applying automated image analysis of static intravital images, we detected dDC-to-MC interactions (sensitivity, 90%; precision > 99%) and evaluated the fraction of interacting MCs in each z-stack relative to the total MC number

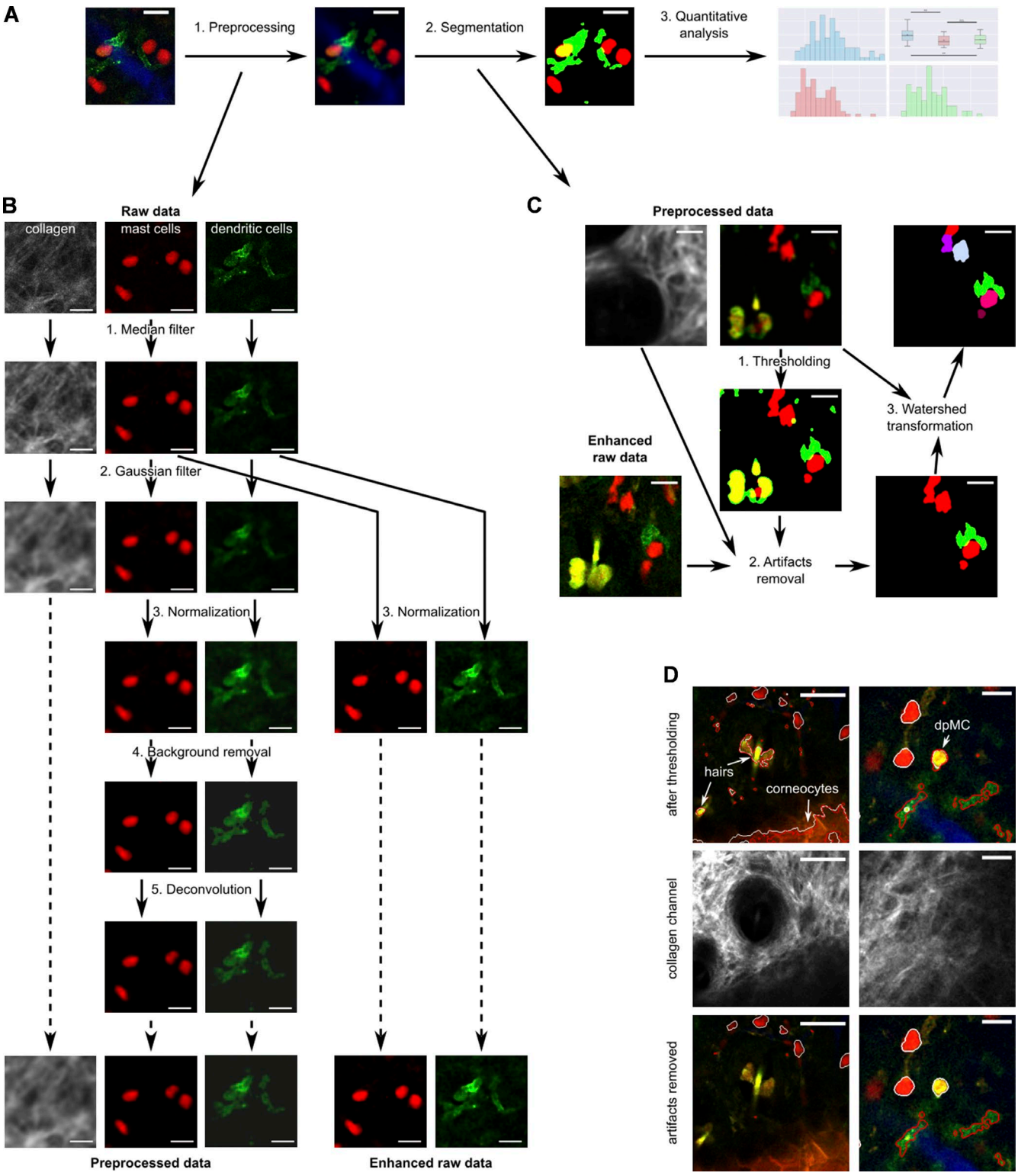

Figure 1. **Image analysis workflow.** (A) Overview of image analysis. (B) Preprocessing workflow. (C) Segmentation workflow. (D) Using the collagen signal (second harmonic generation) for classification between autofluorescence artifacts and GFP$^+$RFP$^+$MCs. Red channel refers to MCs, green channel refers to DCs, blue channel shows blood vessels, and gray channel shows collagen. Bars: (A–C and D [right]) 20 µm; (D, left) 50 µm. See also Fig. S1.

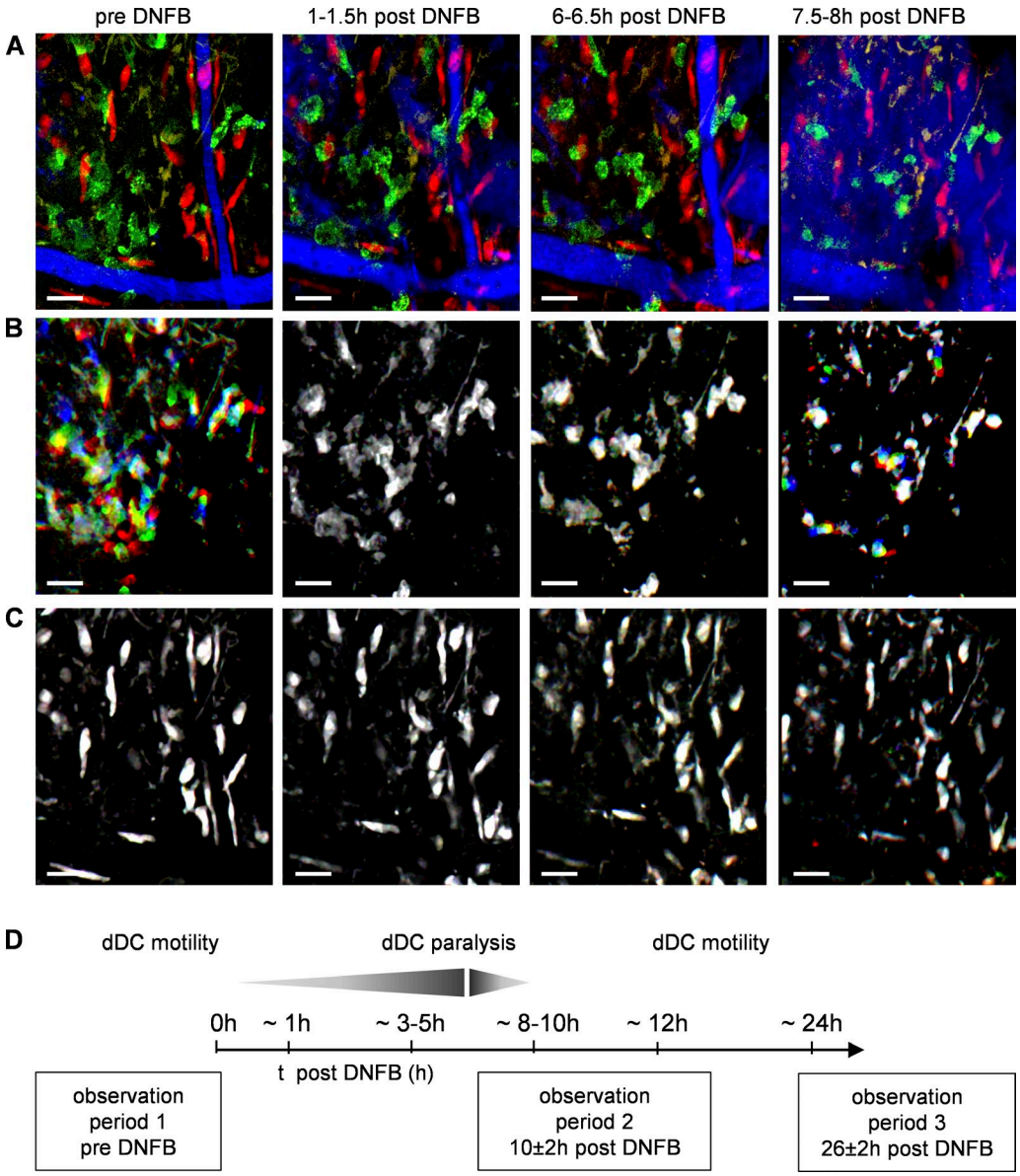

Figure 2. **Dermal DC paralysis and remobilization in responses to DNFB.** (A) Maximum intensity projection DC^{GFP}/MC^{RFP} mouse ear skin representing DCs (green), MCs (red), and blood vessels (blue) before and after DNFB administration at one time point of the corresponding 30-min time-lapse series (Video 1). Bars, 30 µm. (B and C) Kinetic overlay of the DC (B) and MC (C) channel at three consecutive time points (1, 15, and 30 min). Motile cells are colored and immobile cells are white. Bars, 30 µm. (D) Determination of observation time frames according to DC motility. For detailed analysis of MC motility in the determined time frames, see Fig. 3.

before DNFB, at 10 ± 2 h, and until 26 ± 2 h after DNFB administration. Regions of interest (ROIs) were chosen blindly and randomly dispersed in the DC^{GFP}/MC^{RFP} mouse ear skin. We found the fraction of MCs interacting with dDCs to be significantly increased upon skin inflammation, in particular, at the early stage of inflammation after DC remobilization at 10 ± 2 h after DNFB (Fig. 4 C).

By means of intravital time lapse series and computational analysis of interaction parameters over time, we identified distinct qualities of dDC-to-MC cellular communication at various stages of the inflammatory response. In steady-state, dDCs scouting the tissue with high velocity passed immobile MCs without pausing or establishing adhesive contacts (Fig. 5 A and Videos 5 and 6). More resting dDCs appeared to be in passive contacts to closely positioned MCs but with limited active and dynamic cell overlaps (Fig. 4 B). In the early time range of inflammation after dDC remobilization, at 8 to 12 h after DNFB challenge, migrating dDCs intensively and dynamically scanned the surface of stationary MCs (Fig. 5 B, and Videos 7 and 8). With

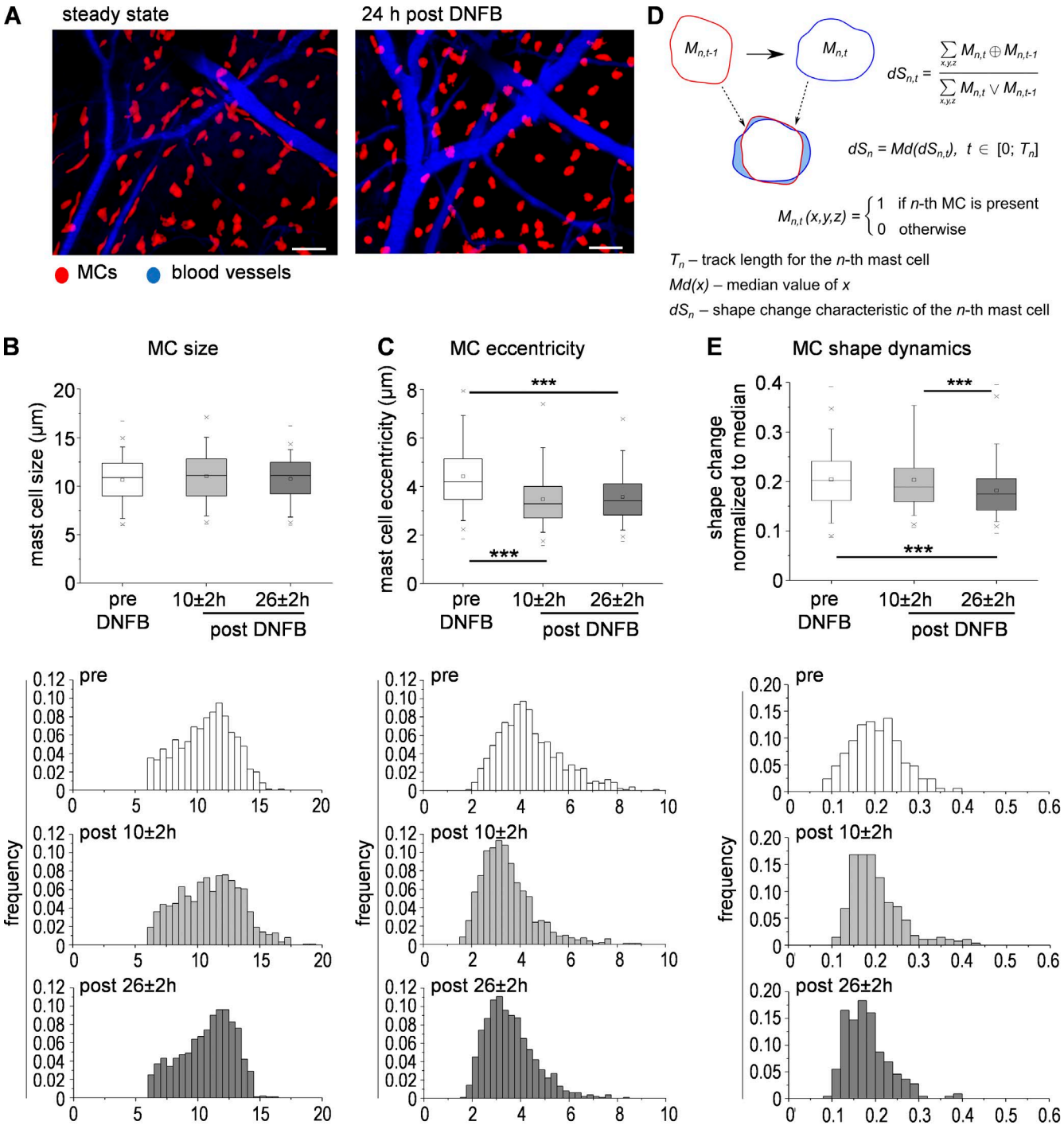

Figure 3. **DNFB-driven skin inflammation induced changes in MCs shape and dynamics.** (A) Intravital multiphoton imaging of MC^{RFP} reporter mouse ear skin before and 24 h after DNFB administration, MIP. Bars, 50 µm. (B and C) Computed quantification of the MC size (B) and eccentricity (C) in randomly chosen ROI z-stacks of DC^{GFP}/MC^{RFP} mice before (n = 102 z-stacks, 8652 cells) and after DNFB (n = 30 z-stacks each, 1,951 and 2,211 cells). Histograms represent the normalized number of MCs with a certain size or eccentricity. (D and E) Dynamic change in MC shape over time of observation in time-lapse series of DC^{GFP}/MC^{RFP} mice ear skin before (n = 168 cell tracks) and after DNFB administration (n = 279 and 218 cell tracks). Histograms represent the normalized number of cell tracks with a certain shape change dynamic of MCs. ***, $P < 0.001$.

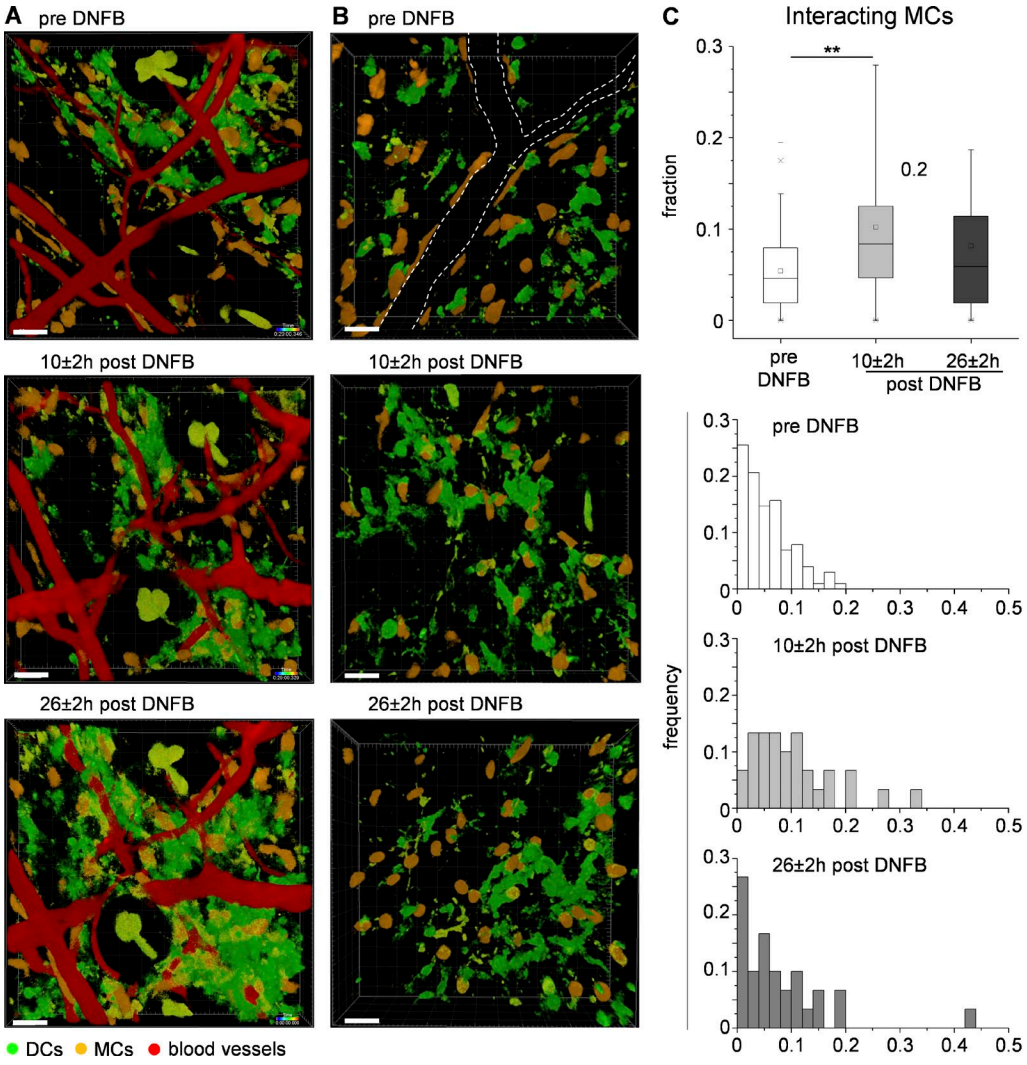

Figure 4. **DCs dynamically cross talk with MCs upon skin inflammation.** Intravital multiphoton imaging of DC^{GFP}/MC^{RFP} mouse ear skin before and after DNFB administration, 3D rendered z-stack. Bars, 40 µm. (A) Longitudinal and side-matched imaging. (B) Dashed line indicates a blood vessel and refers to Videos 2, 3, and 4. (C) Computed quantification of the fraction of MCs interacting with dDCs in randomly chosen z-stacks before (n = 102) and after DNFB administration (n = 30 each). Histograms represent the normalized number of z-stacks with a certain fraction of interacting MCs. **, P < 0.01.

ongoing inflammation (time range of 14 to 24 h after DNFB challenge), dDCs remained in close connection to their target MCs, forming extensive and long-lasting contact zones (Fig. 5, C and D; and Videos 9, 10, 11, and 12). Based on time-lapse series, two dynamic parameters of dDC-to-MC contacts were computed: the contact ratio representing the contact duration normalized to the total time of observation, and the change in DC/MC overlap over time (Fig. S2). Proving the formation of long-lasting and conformal interaction zones, the computed durations of dDC-to-MC contacts have gradually increased with ongoing inflammation as compared with steady-state (Fig. 5 E). A high fraction of DC-to-MC pairs (25.5%) even displayed a contact ratio of 1.0, representing a tight connection over the whole observation time (Fig. 5 E). Correspondingly, the dDC/MC overlap change over time was decreased toward the late inflammation phase of 26 ± 2 h after treatment.

DC-to-MC protein transfer via physical contact zones

Surprisingly, we observed that the extensive physical interactions between DCs and MCs ultimately culminated in the transfer of DC cytoplasmic material to MCs. Beginning ∼18 h after DNFB administration, we monitored the occurrence of originally DC-restricted GFP inclusions within the cell body of RFP^+ MCs (Fig. 6, A and B). Importantly, the GFP^+RFP^+ double-positive MCs were detected in all DC^{GFP}/MC^{RFP} animals after DNFB-induced skin inflammation but never in nonstimulated conditions (Figs. 6 A and 7 A), DNFB-challenged MC^{RFP} single reporter mice, or diphtheria toxin (DT)–treated and thereby DC-depleted

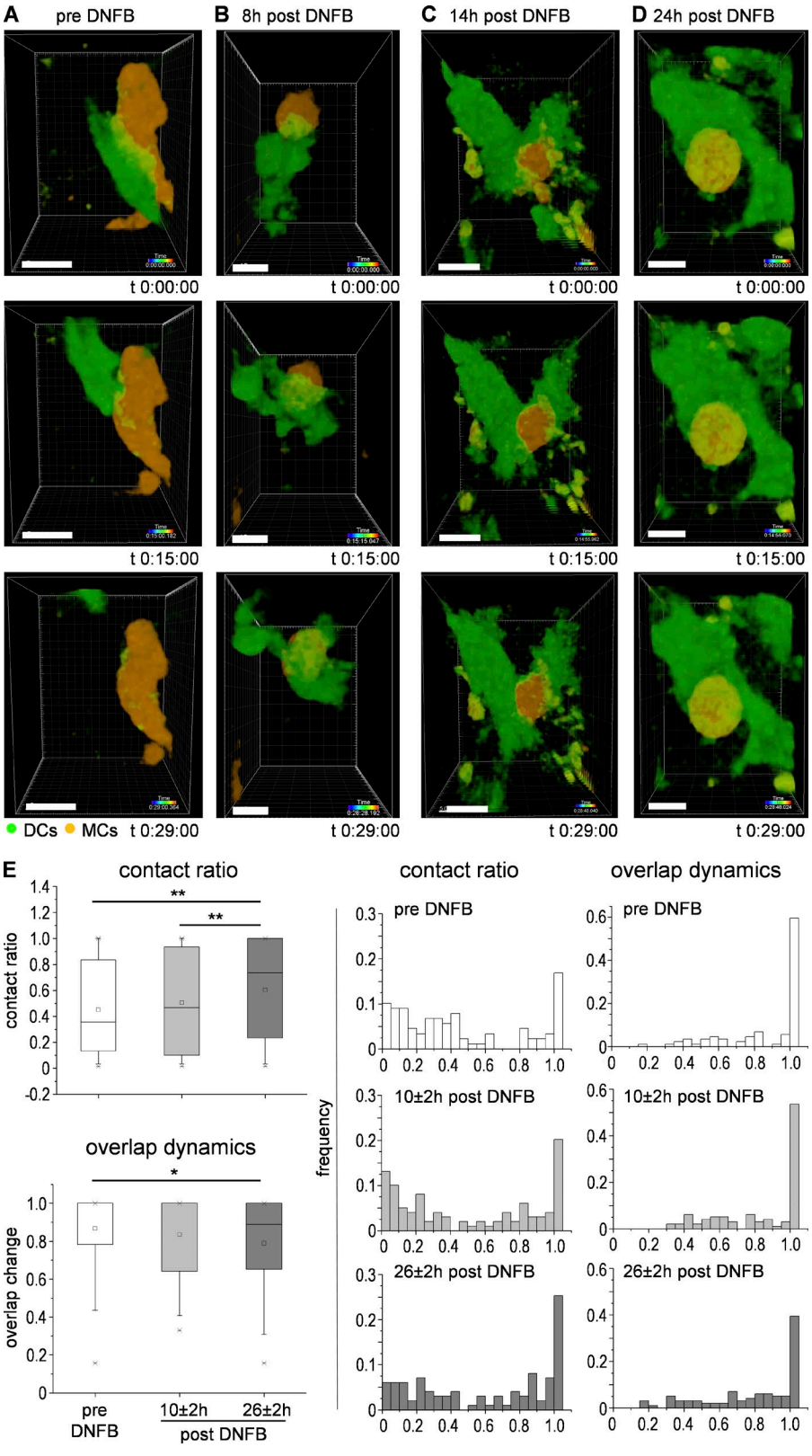

Figure 5. **DC-to-MC communication shifts from dynamic scanning to firm and long-lasting contacts in the progression of skin inflammation.** (A–D) Sequences of intravital time-lapse series (3D-rendered z-stack) of DC/MC pairs before and after DNFB administration. Bars, 10 µm. Refers to Videos 5, 6, 7, 8, 9, 10, 11, and 12. (E) Computed quantification of DC-to-MC contact duration normalized to observation time (contact ratio) and DC/MC overlap change over time before (n = 50 cell tracks) and after DNFB administration (n = 89 [10 ± 2 h], n = 99 [26 ± 2 h]). Histograms represent the normalized number of cell tracks with a certain contact ratio or overlap change. *, P < 0.05; **, P < 0.01.

DC^{GFP}/MC^{RFP} mice (not depicted). Regions of GFP^+RFP^+ MCs were found in variable size and number per DNFB-treated ear skin area, most likely because of varying hapten penetration depths and mouse susceptibility (that may depend on hair cycle, skin integrity, cutaneous scratches, and other unswayable parameters). In strongly responding mice, numerous MCs in large areas displayed a high extent of GFP inclusion with a further gradual increase until 48 h (Fig. 7, B and C). The measurement of the fluorescence emission spectra of various regions in GFP^+RFP^+ MCs in single z-planes revealed demarcated pure GFP inclusions within RFP-expressing MCs, indicating an intercellular protein transfer from dDCs to MCs (Fig. 6 C). Moreover, the single z-plane time lapse series of a DC-to-MC communication depicted in Fig. 5 D and Video 13 proved the transfer of GFP^+ vesicles from the adhered DC into the RFP^+ MC via the DC-to-MC contact zone. In the time range of 48 h to 5 d after DNFB administration, the GFP emission faded within the RFP^+MCs (although the RFP emission did not), suggesting the degradation of GFP^+ inclusions (Figs. 6 A and 7 D). The automated image analysis of randomly chosen ROIs enabled objective evaluation of GFP^+ inclusion in MCs by computing the median ratio of GFP to RFP signals of each MC. Based on this parameter, the double-positive (GFP^+RFP^+) MCs were automatically detected (sensitivity, 82%; precision, 90%), and the fraction of GFP-bearing MCs was computed in each z-stack as the number of GFP^+RFP^+ MCs normalized by the total RFP^+ MC number. This fraction, although diversely sized as explained above, proved to be significantly higher after DNFB challenge as compared with steady-state (Fig. 6 E). When calculating inside responding lesions, we detected even up to 40% of MCs, on average, bearing DC-derived GFP inclusions in addition to RFP (Fig. 6 F).

MCs acquire MHC class II (MHCII) complexes and antigen-presenting competences via DC-to-MC communication

To evaluate whether the DC-to-MC protein transfer includes DC-derived complexes, we generated haplotype mismatch bone marrow (BM) chimera mice, hereafter referred to as SJL/J^{B6}. In brief, irradiated SJL/J recipient mice carrying the MHCII haplotype $H2^s$ and the congenic leukocyte marker CD45.1 were adoptively transferred with BM of C57BL/6 donor mice expressing the MHCII $H2^b$ haplotype and CD45.2 (Lyon and Searle, 1989; Fig. 8 A and Fig. S3; detailed in Materials and methods). In SJL/J^{B6} mice, the radiosensitive recipient DCs ($CD45.1^+$) were replaced by >90% by C57BL/6 donor DCs representing $H2^b$ MHCII and CD45.2 expression (Fig. 8 B). In contrast, >96% of dermal MCs were resistant to irradiation and remained of recipient $CD45.1^+$ genotype, even under inflammatory conditions (Fig. 8 C). In non-transferred SJL mice, MCs exclusively expressed the congenic marker CD45.1 and showed no binding of antibodies directed against the C57BL/6-restricted congenic marker CD45.2 or H^{2b} haplotype MHCII proteins (Fig. 8 D; gating for assessment of CD45.2 and H^{2b} expression). After BM transfer and DNFB-induced skin inflammation, >20% of gated $CD45.1^+$ recipient MCs additionally expressed CD45.2 and MHCII proteins of the $H2^b$ haplotype, proving the transfer of these proteins from donor DCs to recipient MCs (Fig. 8, E and F).

We next questioned whether dDC-donated $H2^b$ MHCII complexes are transferred to the MC surface in a functionally active form. Consequently, DCs would equip the target MCs with the capacity to prime allogeneic SJL/J T cells because of T cell receptor recognition of the nonself $H2^b$ MHCII. SJL/J^{B6} chimeras were generated as described, and DC-to-MC communication was initiated by DNFB-triggered skin inflammation. 24 h after DNFB administration, $CD45.2^+H2^{b+}$ donor DCs and $CD45.1^+$ recipient MCs were FACS-sorted from inflamed ear skin and co-cultured with CFSE-labeled SJL/J T cells (Fig. 9 A). The induction of SJL/J T cell proliferation by equal numbers of SJL/J^{B6} skin DCs and MCs was assessed by means of CFSE dilution in comparison to syngeneic (haplotype matched) SJL/J skin DCs and MCs as negative control and allogeneic (haplotype mismatched) C57BL/6 DCs as positive control. SJL/J^{B6} skin DCs induced a pronounced SJL/J $CD4^+$ T cell proliferation, which was only slightly reduced as compared with C57BL/6 DCs (Fig. 9 B). Most interestingly, 100% pure $CD45.1^+$ recipient MCs sorted from inflamed ear skin of SJL/J^{B6} chimeras initiated a SJL/J $CD4^+$ T cell proliferation (31.8 ± 8.5% of total $CD4^+$ T cells) that was even significantly higher than proliferation evoked by sample-matched skin DCs activated in vivo under the same conditions (Fig. 9 C and Fig. S4). Importantly, we determined a linear correlation between the degree of $CD4^+$ T cell proliferation and the extent of MCs bearing $H2^b$ MHCII surface molecules with a Pearson's correlation coefficient of 0.9 (Fig. 9 D). We further quantified the allogeneic effector T cell cytokine response promoted by the $H2^b$ MHCII -loaded MCs in co-culture supernatants in comparison to T cell–DC co-cultures. The SJL/J $CD4^+$ T cell proliferation induced by allogeneic stimulation with MCs sorted from SJL/J^{B6} chimera inflamed ear skin was associated with a significant release of IFN-γ, IL-6, TNF, and IL-12p70 as compared with SJL/J T cell co-cultures with MCs from SJL/J (nonchimeric) mice (Fig. 9 E). Surprisingly, the level of TNF and IL-6 production elicited upon SJL/J T cell co-culture with SJL/J^{B6} chimera MCs was dramatically potentiated as compared with the levels of SJL/J T cell co-culture with SJL/J^{B6} chimera skin DCs and B6 spleen DCs. In contrast, production of IL-4 and IL-5 was not initiated by SJL/J T cell co-culture with SJL/J^{B6} chimera MCs and thereby was significantly lower than IL-4 and IL-5 levels of co-culture supernatants of SJL/J T cells with SJL/J^{B6} chimera skin DCs (Fig. 9 E). Collectively, we demonstrated by means of haplotype mismatch BM chimeras that inflammation-induced DC-to-MC communication equips MCs with DC-donated $H2^b$ haplotype MHCII complexes and antigen-presentation competences resulting in allogeneic T cell priming with a distinct cytokine signature.

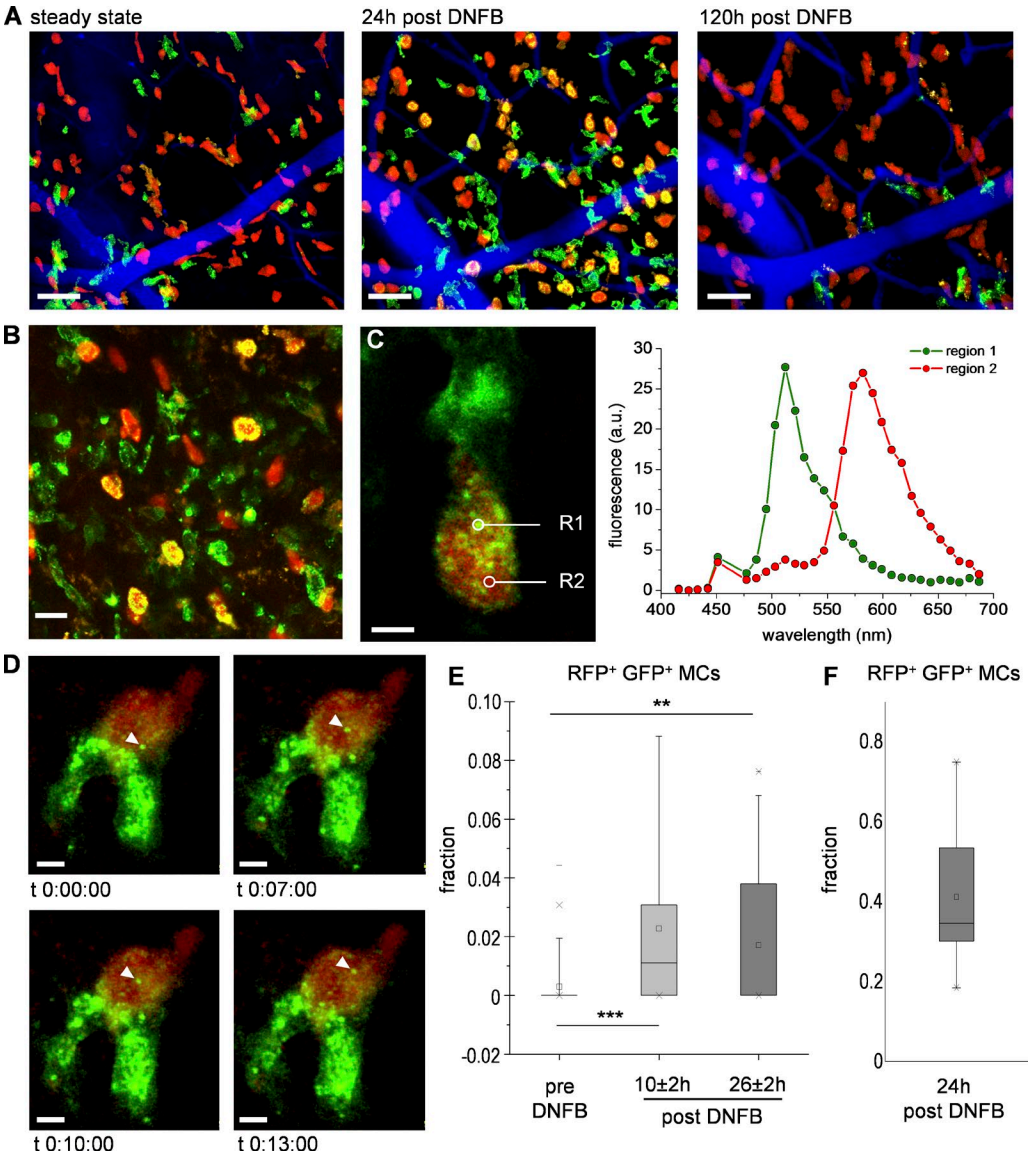

Figure 6. **DC-to-MC interactions culminate in DC protein transfer to MCs.** Intravital imaging of DC^{GFP}/MC^{RFP} mouse ear skin (A) before and after DNFB, MIP. Bars, 50 µm. (B) MIP, 24 h after DNFB. Bar, 20 µm. (C) Fluorescence emission spectra of two separate intracellular regions in a single image z-plane of a GFP^+RFP^+MC. Bar, 5 µm. (D) Single z-plane imaging of GFP vesicle transfer (white arrowheads) from GFP^+DC into RFP^+MC 24 h after DNFB. Bars, 5 µm. Refers to Video 13. (E) Random analysis of GFP^+RFP^+ MCs before (n = 102) and after DNFB (n = 30, each). (F) Quantification of GFP^+RFP^+MCs at 24 h after DNFB focused on responsive lesions (n = 16). **, $P < 0.01$; ***, $P < 0.001$.

DC-to-MC communication contributes to T cell–driven adaptive skin inflammation

Next, we investigated whether DC-to-MC communication contributes to T cell–driven skin inflammation. We used CD11c-Cre mice bred to the iDTR line (Buch et al., 2005), in which a simian DT receptor is expressed selectively in Cre recombinase-expressing cells deleting a loxP-flanked stop element. Because WT mouse cells are resistant to DT, only DCs were expected to be sensitive to DT-induced cell death in CD11c-Cre^+ $iDTR^+$ offspring. Indeed, we proved that intradermal (i.d.) injection of DT into the ear resulted in efficient DC depletion in CD11c-Cre^+ iDTR already at 4 h and lasting for at least 48 h after DT treatment (Fig. 10 C), whereas DC numbers in DT-treated Cre^- controls and MC numbers in DT-treated CD11c-Cre^+ mice and Cre^- controls were not affected (Fig. 10, C and D). CD11c-Cre iDTR mice were first sensitized with DNFB on the ear to induce innate skin inflammation and subsequently treated with DT as follows: (1) CD11c-Cre^- iDTR, DT-treated at 48 h after DNFB, representing full DC-to-MC communication and DC presence; (2) CD11c-Cre^+ iDTR, DT-treated 48 h after DNFB (after DC-to-MC communication) to assess the

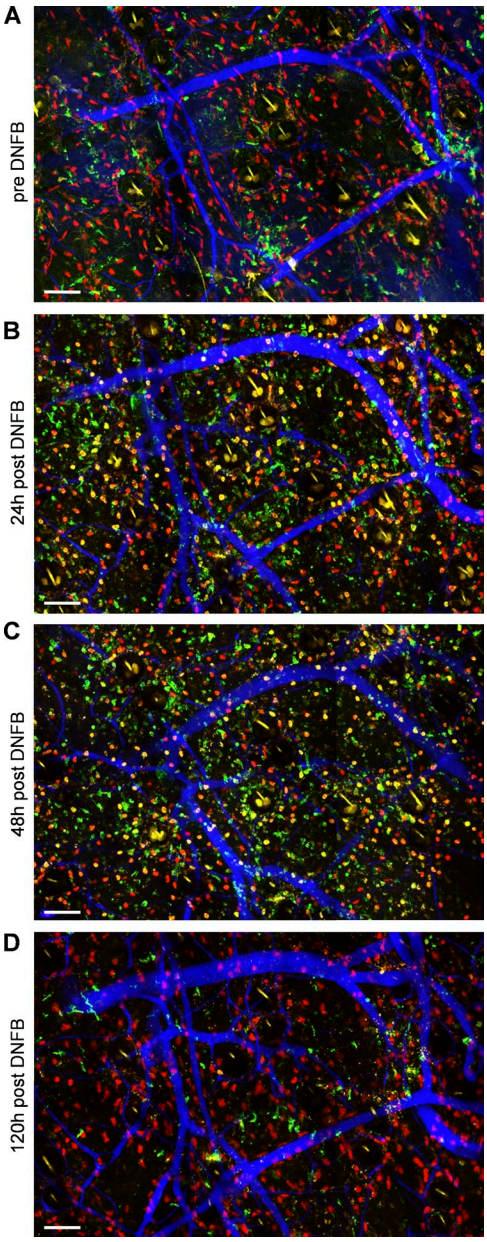

Figure 7. **Skin inflammation-induced DC-GFP transfer to MCs is followed by complete degradation of GFP inclusions on site.** (A–D) Longitudinal and side-matched intravital imaging of DC^{GFP}/MC^{RFP} mouse ear skin before and after DNFB administration. Bars, 100 µm. MCs are shown in red, DCs in green, and blood vessels in blue.

contribution of DC-instructed MCs in absence of DCs; and (3) CD11c-Cre^{+}iDTR, DT-treated at 4 h after DNFB and thereby impeding DC-to-MC communication (Fig. 10 A). Effector T cell–driven skin inflammation was induced by an adoptive transfer of equal numbers of LN T cells pooled from DNFB-sensitized WT mice into the DNFB-sensitized ear skin of CD11c-Cre iDTR recipient groups 72 h after DNFB to exclude DC depletion effects on recipient T cell priming and homing, and quantified as ear swelling. We found that the adoptive transfer of DNFB-primed T cells into DNFB-sensitized recipient ear skin caused a massive adaptive response in CD11c-Cre^{-} mice (group 1) in the time range of 24 to 96 h after injection (Fig. 10 B). The adaptive ear swelling response was only moderately reduced in CD11C-Cre^{+} iDTR mice, where DCs were depleted after DC-to-MC communication (group 2) when compared with DC-proficient CD11c-Cre^{-} mice (group 1). Importantly, compared with DC-proficient mice (group 1) but also to DC-depleted mice (group 2), the skin inflammation was dramatically and significantly impaired in recipient mice of group 3, where DCs were depleted before DC-to-MC communication, implying the absence of DC-instructed MCs (Fig. 10 B). These findings indicate a critical contribution of DC-to-MC communication in vivo as reflected by the quantitative impact on the subsequent T cell–driven skin inflammation.

Substantial role for MC endogenous and acquired MHCII complexes in the pathology of CHS

We further questioned the relevance of MC MHCII complexes and antigen-presenting capacity in the pathology of CHS. To this end, we used MC-deficient Mcpt5-Cre^{+} $RDTA^{+/+}$ mice, in which connective tissue–type MCs (CTMCs) are constitutively depleted because of an intrinsic expression of DT (Voehringer et al., 2008; Peschke et al., 2014, 2015), and reconstituted one ear with ex vivo enriched CTMCs from WT mice and one ear with CTMCs lacking MHCII from $MHCII^{-/-}$ mice (Fig. 10 E; Madsen et al., 1999). CHS was performed 4 wk after reconstitution, and the adaptive T cell–driven CHS response was assessed by ear swelling and skin cytokine analysis. Importantly, we found that the ear swelling response was markedly diminished in the absence of MC-specific MHCII expression at 24 h (not depicted) and 48 h (Fig. 10 F) after hapten administration, demonstrating the functional relevance of MC antigen presentation to disease severity of CHS. To additionally discriminate the relevance of endogenous MC-MHCII vs. MHCII acquired by MCs via the interaction with DCs, we crossed the Mcpt5-Cre RDTA line to the CD11c-eGFP/DTR line, allowing depletion of conventional $CD11c^{+}$ DCs by i.d. injection of DT. MC-deficient Mcpt5-Cre^{+} R-$DTA^{+/+}$ × CD11c-eGFP/DTR mice were reconstituted in one ear with CTMCs from WT and in the contralateral ear with CTMCs from $MHCII^{-/-}$ mice. Mice were sensitized and challenged as described in the Material and methods section, but DCs were depleted by i.d. DT injection either 4 h after challenge to impede DC-to-MC interaction or 48 h after challenge to allow previous MHCII acquisition of MCs from DCs. Most importantly, we found that the ear swelling response of MC-deficient mice reconstituted with $MHCII^{-/-}$ MCs at 24 h (not depicted) and 48 h (Fig. 10 F) after challenge (Fig. 10) was further reduced by impeding DC-to-MC interaction and acquisition of DC-restricted MHCII by MCs. Moreover, the tissues levels of IL-2 and IL-18 were significantly reduced in mice lacking MC-MHCII and in mice with impeded DC-to-MC inter-

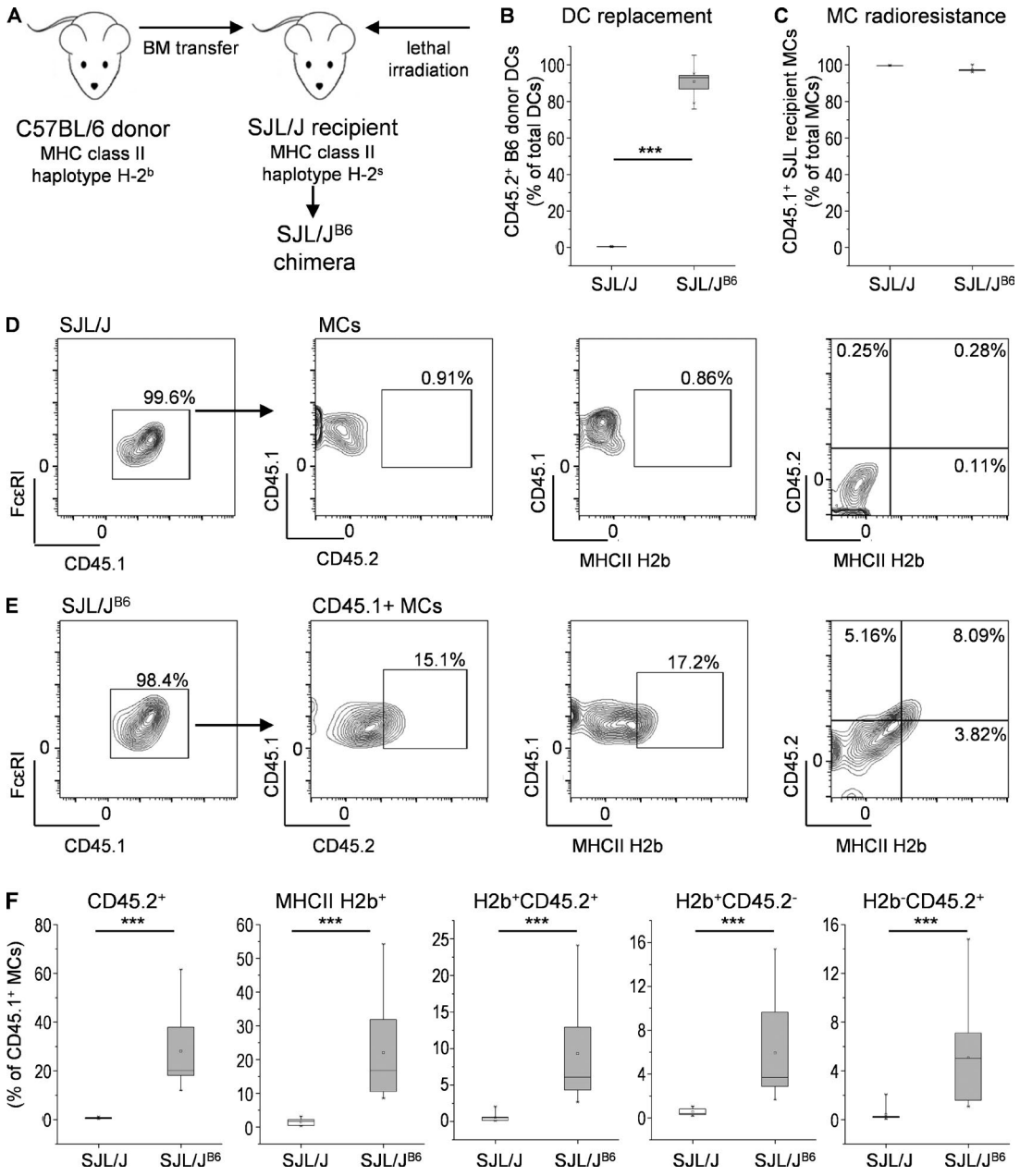

Figure 8. **MCs incorporate donor DC-derived H2^b MHCII protein complexes.** (A) SJL/J^{B6} BM chimera were generated by BM transplantation from C57BL/6 donor mice (CD45.2$^+$ H2^b MHCII) to SJL/J recipients (CD45.1$^+$ H2^s MHCII). (B) CD45.2$^+$ expression on skin DCs from SJL/J mice (n = 6) and SJL/J^{B6} BM chimera 24 h after DNFB (n = 8) was assessed by flow cytometry. (C) CD45.1$^+$ expression on skin MCs from SJL/J mice (n = 6) and SJL/J^{B6} BM chimera 24 h after DNFB (n = 8). (D–F) Surface CD45.2 and intracellular H2^b MHCII expression by CD45.1$^+$ recipient ear skin MCs (c-kit$^+$FcεRI$^+$) of SJL/J mice (D) and SJL/J^{B6} BM chimera (E) 24 h after DNFB was measured by flow cytometry and quantified as box plot (F). ***, P < 0.001.

action caused by prior DC depletion (Fig. 10 G), suggesting that MC antigen presentation may promote T cell survival at the site of inflammation.

DISCUSSION

The close proximity of DCs and MCs in peripheral tissues at environmental interfaces allows for a response of DCs to soluble MC mediators as well as for the formation of cell–cell contacts. We and others demonstrated i*n vitro* that direct contacts to MCs enhance DC maturation and subsequent T cell stimulation (Kitawaki et al., 2006; Dudeck et al., 2011b; Otsuka et al., 2011; Carroll-Portillo et al., 2012). Recently, Joulia et al. showed FcR-triggered MC contacts to IgE- or IgG-bearing B cells resulting in a vectorial exposure of gran-

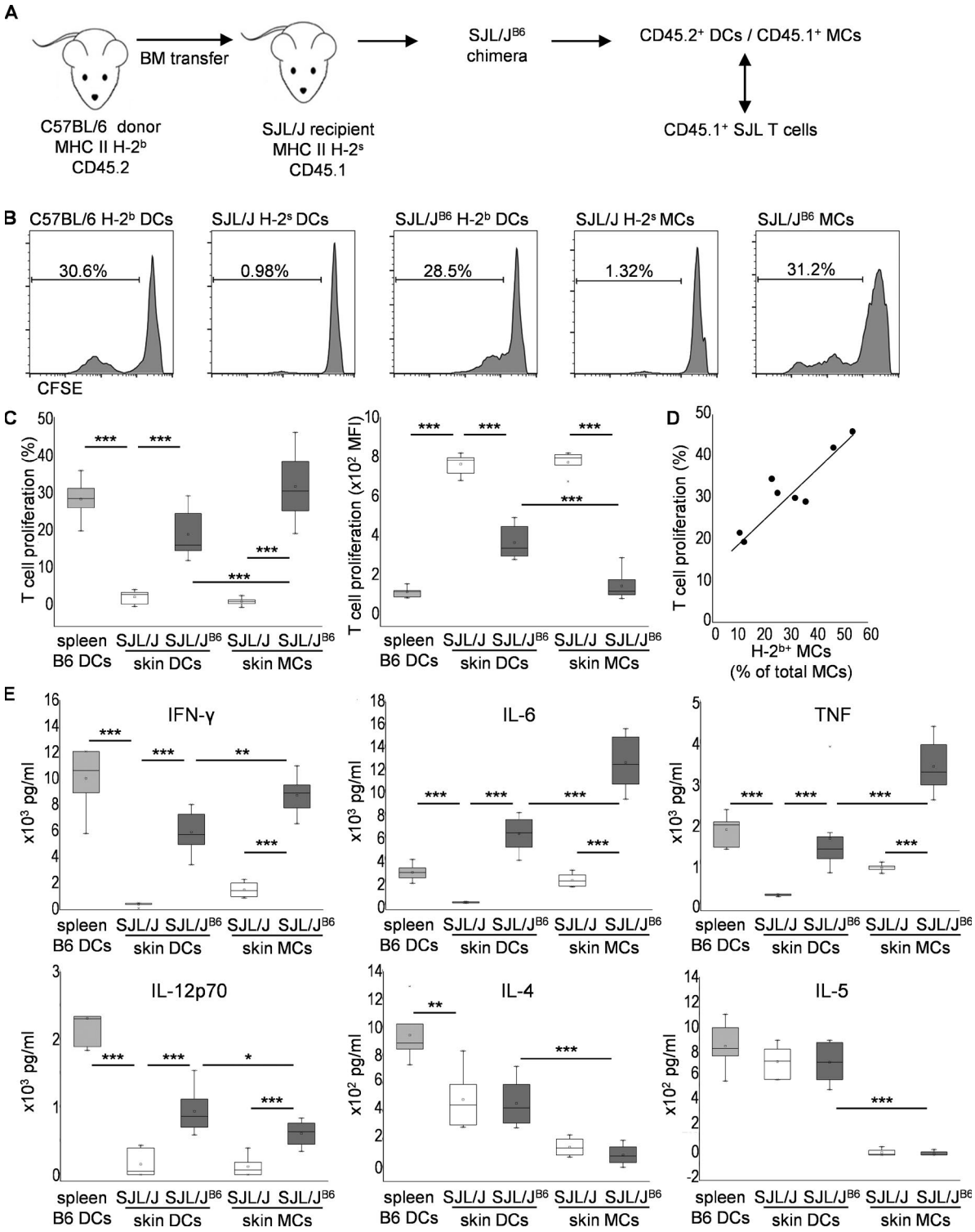

Figure 9. **DC-instructed MCs efficiently induce ex vivo allogeneic T cell priming.** (A) SJL/J^{B6} chimera were generated by lethal irradiation of SJL/J recipient mice and transfer of BM cells from C57/BL6 donor mice. DC-to-MC communication was induced by DNFB administration onto ear skin of SJL/JB6 chimera mice or control SJL/J mice, and DCs and MCs were sorted from ear skin 24 h after DNFB. CFSE-labeled SJL/J T cells were cocultured with DCs (CD45.2$^+$CD11c$^+$H2b$^+$) and MCs (CD45.1$^+$c-kit$^+$FcεRI$^+$) sorted from ear skin of SJL/J^{B6} chimera mice ($n = 9$) or SJL/J control mice ($n = 6$) 24 h after DNFB, or C57BL/6 spleen DCs ($n = 6$) as positive control. (B and C) T cell proliferation was assessed as CFSE dilution (B) and quantified as proliferated T cell fraction from total T cells and as mean fluorescence intensity (MFI; C). (D) The proliferated T cell fraction was plotted versus the H2^b-expressing MC fraction to assess parameter correlation. (E) Cytokines released upon SJL/J T cell co-culture with DCs and MCs were quantified in the co-culture supernatant by bead-based multiplex assay. *, $P < 0.05$; **, $P < 0.01$; ***, $P < 0.001$.

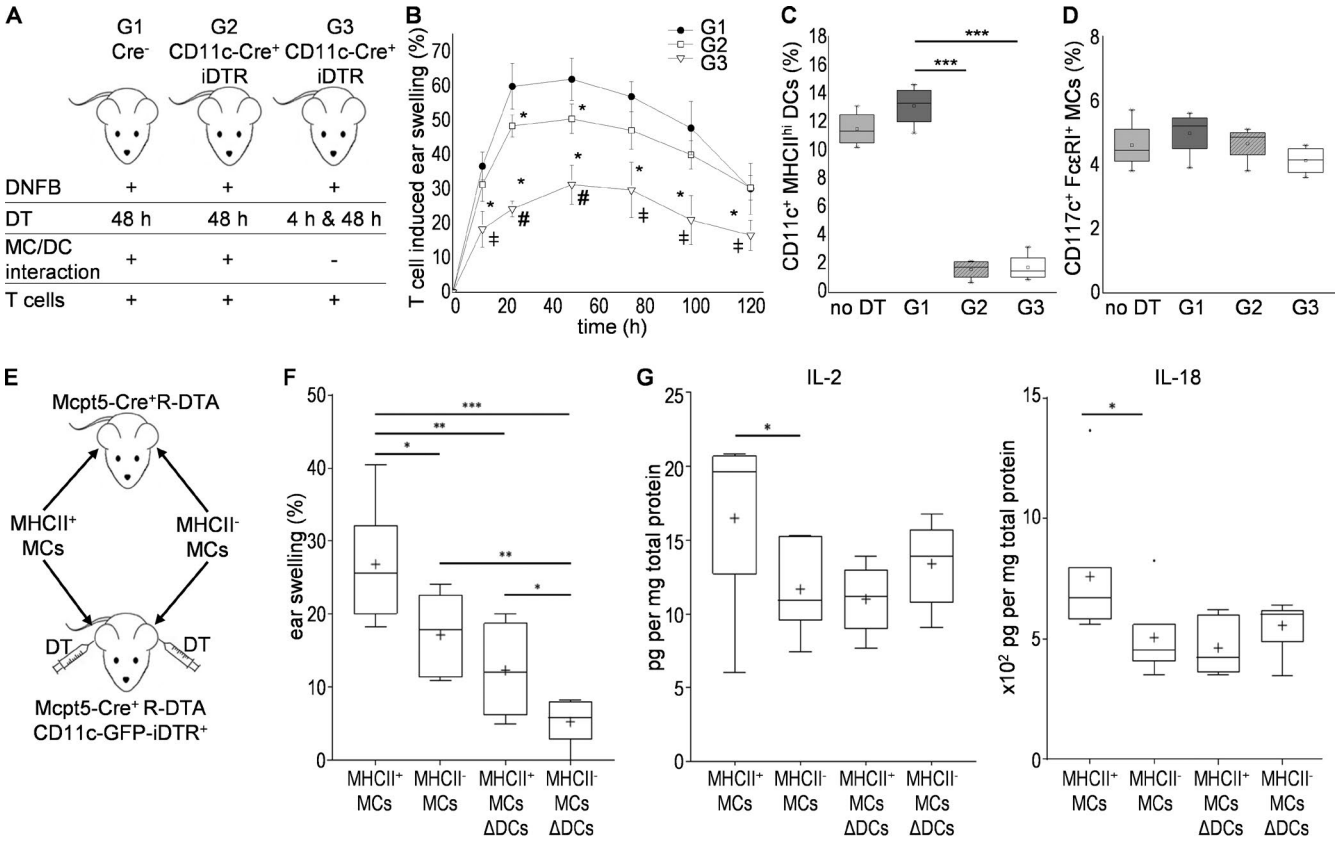

Figure 10. **DC-to-MC communication critically contributes to hapten-specific T cell–induced skin inflammation.** (A) Skin inflammation was induced by i.d. injection of T cells from DNFB-sensitized WT donor mice into DNFB-treated ear skin of recipient mice as follows: group G1: CD11c-Cre$^-$ iDTR control mice treated with DT 48 h after DNFB; group G2: CD11c-Cre$^+$ iDTR mice treated with DT 48 h after DNFB; and group G3: CD11c-Cre$^+$ iDTR mice treated with DT at 4 h and 48 h after DNFB. (B) T cell–induced ear swelling was measured at the indicated time points. Data are represented as mean ± SD. *, $P < 0.005$ related to group 1; ǂ, $P < 0.05$ related to group 2; #, $P < 0.005$ related to group 2; $n = 8$/group. (C and D) CD11c$^+$MHCII^{hi} DC numbers (C) and CD117$^+$FcεRI$^+$ MC numbers (D) were quantified 24 h after last DT injection by flow cytometry in comparison to not DT-treated Cre$^-$ controls. ***, $P < 0.001$; $n = 5$/group. (E) MC-deficient Mcpt5-Cre$^+$ R-DTA$^+$ mice and Mcpt5-Cre$^+$ R-DTA$^+$ × CD11c-eGFP/DTR mice were reconstituted with WT CTMCs in one ear and MHCII$^{-/-}$ CTMCs in the contralateral ear ($n = 7$/group). 4 wk after reconstitution, recipient mice were sensitized and challenged with DNFB. In Mcpt5-Cre$^+$ R-DTA$^+$ × CD11c-eGFP/DTR mice, DCs were locally depleted by i.d. injection of DT into the ear pinnae 4 h after DNFB. (F and G) Ear swelling was measured 24 h and 48 h after DNFB (F), and cytokines were quantified in protein extracts of challenged ear skin 48 h after DNFB (G) using a bead-based multiplex assay. *, $P < 0.05$; **, $P < 0.01$; ***, $P < 0.001$.

ules, which the authors termed antibody-dependent degranulatory synapse (ADSS; Joulia et al., 2015; Valitutti et al., 2017). Such a synapse formation between MCs and DCs may allow for the delivery of more concentrated doses of soluble mediators. Indeed, Carroll-Portillo demonstrated that activation of MCs through FcεRI cross-linking triggers the formation of stable cell–cell interactions with immature DCs in vitro, which they called synapses (Carroll-Portillo et al., 2015). Importantly, this synapse formation facilitates the transfer of internalized MC-specific antigen from MCs to DCs, which is ultimately processed and presented by DCs and can activate T cells. MC-DC interactions in peripheral tissues such as the skin have been speculated based on the observation of static contacts in tissue sections (Carroll-Portillo et al., 2015). However, a dynamic or even directed cell-to-cell cross talk has so far never been proven in vivo. Moreover, the effect of such cell-to-cell contacts on MCs has never been addressed. In this study, we show for the first time a highly dynamic communication between dermal DCs and MCs in vivo and in real-time that is specifically evoked by skin inflammation. Combining intense longitudinal multiphoton imaging and quantitative image analyses of a high number of randomly chosen ROIs, we prove the cross talk to be significantly elevated upon inflammation instead of being by-chance interactions caused by the close proximity within the complex tissue. Importantly, once initiated, the DC-to-MC communication shows a constant development during the time course of immune response. On one hand, the number of DC/MC interactions increases with ongoing inflammation. On the other hand, this innate-to-innate immune communication progresses in quality from dynamic scanning of the MC surface by DCs to the establishment of extensive and long-lasting MC/DC

contacts indicating innate-to-innate immune synapse-like contacts. Surprisingly, these synapse-like firm contacts ultimately culminate in a protein transfer from dermal DCs to the tissue resident MCs that includes MHCII molecules. Given the transfer of the cell surface molecules MHCII and CD45, MCs may extract membrane patches from the DCs through the innate-to-innate synapse-like contacts in a trogocytosis mechanism. The phenomenon of trogocytosis termed by Hudrisier and colleagues describes a dynamic transfer of membrane patches within minutes after conjugate formation between two cells that might reflect an arrangement of leukocytes to deliver defense competences against pathogens (Huang et al., 1999; Hudrisier et al., 2001; Stinchcombe et al., 2001; Joly and Hudrisier, 2003). However, the observation of vesicle-like structures appearing within the MCs via the synapse-like contacts to DCs may also suggest an endocytosis-like mechanism or tunneling nanotubes (Watkins and Salter, 2005; Gerdes and Carvalho, 2008). Further detailed analysis of the DC-to-MC synapses and resulting protein exchange is required to discriminate the underlying mechanism. Whatever the mechanism might be, "cross-dressing," meaning the intercellular transfer of MHC molecules, has been described not only between APCs and T cells but also between other cell types including APCs–APCs, tumor cells–APCs, and epithelial cells–APCs (Campana et al., 2015). Importantly, Dolan et al. demonstrated that upon transfer, DCs acquire fully functional MHC–peptide complexes, enabling the "cross-dressed" DCs to present the acquired peptide (Dolan et al., 2006a,b).

Despite MCs and dermal DCs both being skin resident innate cells, they undertake distinct defense responsibilities. DCs link innate to adaptive immunity by migrating from infected or damaged peripheral tissues to draining LNs, where they present peripherally engulfed antigens to prime antigen-specific naive T cells to effector T cells. However, the adaptive immunity-priming task of DCs in draining LNs necessarily implies their absence in the periphery during encounter of the corresponding antigen-specific effector T cells. MCs concurrently promote DC functions upon tissue inflammation but remain in the periphery. Given the DC-to-MC synapse-like contact formation and DC protein transfer to MCs before leaving the skin, we speculated that MCs shall be equipped by DCs to maintain the line of defense during the DC underrepresentation in the affected tissue. Consequently, cross-dressing of MCs by DCs with MHC–peptide complexes might transfer the competence of effector T cell restimulation. The polygenic and polymorphic nature of the MHC gene locus ensures the diversity of antigen presentation. However, it also results in structural differences of MHC proteins between different mouse strains that can be detected by haplotype specific antibodies. Using a haplotype mismatch BM transfer, we could indeed prove the transfer of donor DC-derived $H2^b$ haplotype MHCII complexes to the radioresistant MCs before DC migration to draining LNs. Given the extremely long kinetic stability of MHCII–peptide complexes with half-life times of up to 150 h (Lazarski et al., 2005), the transfer would allow for the compensation of DC functions by remaining MCs. T cell acquisition of MHC molecules and bystander ligands from B cells and epithelial cells has been previously demonstrated in vivo by similar approaches of BM chimeras or adoptive T cell transfer experiments (Hudson et al., 1974; Hudson and Sprent, 1976; Sharrow et al., 1981). Here, we for the first time identify MCs as tissue resident innate myeloid target cells for physical DC communication to be equipped with DC donated MHC–peptide complexes. Importantly, we prove the $H2^b$ haplotype MHCII complexes to be transferred from DCs to MCs in a fully functional manner "upgrading" MCs with the capacity to prime allogeneic SJL/J T cells. Moreover, the priming capacity of MCs closely correlates to the extent of transferred $H2^b$ MHCII complexes. Given the fact that only a fraction of MCs, ∼30%, were equipped with DC-derived surface $H2^b$ MHCII, skin MCs emerge as being more efficient in priming $CD4^+$ T cells ex vivo than $H2^b$ skin DCs. Future work will be needed to clarify whether this effect may be attributed to the immature state of nonlymphoid tissue–residing DCs that are known to gain full maturation while migrating to draining LNs (Lanzavecchia and Sallusto, 2001). Otherwise, MCs may carry an optimal intrinsic potential to serve as efficient APCs for the restimulation of effector T cells homing to peripheral tissue as soon as equipped with MHCII–peptide complexes by DCs. In the last decade, it has been suggested that MCs might serve as APCs for T cells. However, recent studies demonstrated that MCs express MHCII upon stimulation with IFN-γ and can serve as resident APCs supporting restimulation of preactivated effector $CD4^+$ T cells in inflamed tissues (Gaudenzio et al., 2009, 2013; Kambayashi et al., 2009). Moreover, Gaudenzio et al. (2013) reported that IFN-γ–primed MCs drive generation of Th22 cells in a TNF- and IL-6–dependent mechanism. Importantly, we herein found that allogeneic T cell priming by skin MCs of haplotype mismatch chimeras was associated with a dramatic production of TNF and IL-6 by either MCs or activated T cells in addition to IFN-γ and IL-12 levels that were comparable to DC/T cell co-cultures. Confirming the study of Gaudenzio et al. (2013), our findings consequently indicate that MCs equipped with priming capacity by DCs evoke a MC-specific cytokine signature that drives effector T cell responses toward a Th17 and Th22 polarization. The "upgrading" of MCs with DC features strongly suggests a distinctive contribution of tissue resident MCs in initiating, maintaining, or amplifying adaptive responses of effector T cells homing to the inflamed skin. In line with the "second touch hypothesis" (Ley, 2014), DCs could be mainly responsible for T cell priming in LNs, whereas MCs might play a key role in driving the end-differentiation and polarization of "antigen-experienced" T cells in the inflamed nonlymphoid tissue where the antigen resides. Most importantly, we herein prove that in addition to cross-dressing of MCs with MHCII–peptide complexes acquired by DCs, MC expression of endogenous MHCII also critically contributes to the severity of T cell responses

during the CHS elicitation phase and may make an even greater contribution to cytokine expression at the sites of inflammation. However, the fact that impeding DC-to-MC exchange by previous DC depletion further decreases CHS severity or effector T cell–driven skin inflammation implicates the functional relevance of acquired MHCII complexes of MCs from DCs. In turn, MCs alone can efficiently restimulate preactivated donor T cells in the absence of DCs when DC-to-MC interaction occurred before. Importantly, proving the MHCII transfer by means of haplotype mismatch does not exclude simultaneous transfer of MHCI or further molecule complexes crucial for antigen presentation or effector T cell restimulation. Several studies have demonstrated that the hapten-specific T cell–driven adaptive immune response during CHS comprises both MHCI-restricted $CD8^+$ T cells and MHCII-restricted $CD4^+$ T cells, but their respective contribution is still not fully understood. Cytoxicity as well as IL-17 and IFN-γ production by $CD8^+$ T cells appear to be the most relevant effector mechanisms causing tissue damage (Bour et al., 1995; Kehren et al., 1999; He et al., 2006; Kish et al., 2009; Zhao et al., 2009) In contrast, $CD4^+$ T cells might play a multifunctional role because they support $CD8^+$ T cell immigration but also provide both effector and regulatory mechanisms (Bour et al., 1995; Fyhrquist et al., 2012). Importantly, recent studies provide novel insights into distinct functions of Th17 cells and Th9 cells in CHS or atopic contact dermatitis that seem to range from proinflammatory to regulatory aspects (Peiser, 2013; Liu et al., 2014; Simon et al., 2014; Martin, 2015). Moreover, MCs have been suggested to execute either a proinflammatory or a protective role depending on the severity of the DNFB-induced CHS reaction (Reber et al., 2017). Of note, an immunosuppressive function of MCs may be in context with the herein observed function as tissue-resident APCs by limiting effector T cell activation during restimulation in the tissue or by stimulating regulatory T cells as a result of the release of IL-10, the extent of which may be regulated dependent on the severity of inflammation.

In summary, we have identified in vivo the targeted and highly dynamic communication between DCs and MCs initiated by inflammatory conditions. Quantification of the physical DC/MC interaction reveals a progression to the formation of extensive and long-lasting innate-to-innate synapse-like contacts culminating in DC-to-MC protein transfer including MHCII complexes. The cross-dressing of residual MCs with DC MHCII facilitates T cell–driven skin inflammation and may ensure the host defense and skin barrier integrity with all functionalities during DC migration to skin-draining LNs.

MATERIALS AND METHODS

Mice

Mcpt5-Cre mice crossed to the R26-tdRFP, R-DTA or CD11c-DTR/eGFP line, and CD11c-Cre mice crossed to the iDTR line, were bred and housed at the Experimental Centre at the Technische Universität Dresden, Medical Faculty Carl-Gustav Carus, under specific pathogen-free conditions. CD11c-DTR/eGFP and CD11c-Cre mice for breeding were purchased from Jackson Laboratories. Mcpt5-Cre mice were provided by A. Roers (Technische Universität, Dresden, Germany), R26-tdRFP by H.J. Fehling (Ulm University, Ulm, Germany), iDTR by A. Waisman (Johannes-Gutenberg University, Mainz, Germany), R-DTA by D. Voehringer (University Clinic, Erlangen, Germany), and $MHCII^{-/-}$ mice (B6.129S2-$H2^{dlAb1\text{-}Ea}$/J) by B. Schröder (Christian-Albrechts University, Kiel, Germany). $CD45.2^+$ C57BL/6 and $CD45.1^+$ SJL/J mice were purchased from Janvier and Charles River, respectively. All mice were of C57BL/6 background. In all experiments, mice were used at the age of 8 to 16 wk. All procedures were in accordance with institutional guidelines on animal welfare and were approved by the Landesdirektion Dresden (24-9168.11-1/2012-38).

Chemicals and reagents

DNFB (1-fluoro-2,4-dinitrobenzene) and hyaluronidase were obtained from Sigma-Aldrich. Liberase TM and DNase I were purchased from Roche. DT was obtained from Enzo Life Sciences. Recombinant murine IL-3 and recombinant rat SCF were obtained from Peprotech. The following mAbs directed against mouse antigens were obtained from eBiosciences: CD117 (clone 2B8), FcεRIα (MAR-1), CD45 (30-F11), CD11c (N418), F4/80 (BM8), MHCII I-A/I-E (M5/114.15.2), MHCII $I\text{-}A^b$ (AF6-120.1), CD45.1 (A20), CD45.2 (104), CD3 (eBio500A2), and CD4 (GK1.5). CFSE was obtained from Molecular Probes (Life Technologies).

CHS

Mice were sensitized with 100 µl 0.5% DNFB in acetone/oil (4:1) on the shaved back skin and challenged 6 d later with 20 µl 0.2% DNFB on the ear (10 µl/ear side). For imaging analysis, 20 µl 0.2% DNFB in acetone/olive oil (4:1) was epicutaneously applied on one side of the ear. Vehicle control mice were treated with the solvent only.

Flow cytometry analysis of skin cells

For preparation of skin cell suspensions, samples of ear skin were cut into small pieces and digested in 1 ml DMEM containing 20 mM Hepes, 0.025 mg/ml Liberase TM, 396 U/ml DNase I, and 0.5 mg/ml hyaluronidase at 37°C, 1400 rpm for 1 h. Samples were passed through a 40-µm sieve and the cell suspension was washed twice with PBS. For flow cytometry analysis, cells were resuspended in PBS/2% BSA and stained with mAbs for 30 min at 4°C. Cell suspensions were washed twice and resuspended in 200 µl PBS/2% BSA. Analysis was done using the Miltenyi MacsQuant flow cytometer with MacsQuant or FlowJo Analysis Software.

MC reconstitution of MC-deficient mice

Peritoneal MCs reflecting CTMCs were obtained from either C57BL/6 WT mice or $MHCII^{-/-}$ mice (B6.129S2-$H2^{dlAb1\text{-}Ea}$/J) as previously described (Dudeck et al., 2011b). In brief, cells from peritoneal lavage of respective donor mice were cul-

tured in RPMI with 10% FCS, 1% penicillin/streptomycin, 10 ng/ml IL-3, and 30 ng/ml SCF. After 48 h, nonadherent cells were carefully removed and replaced by fresh culture medium to enhance the purity of resulting MCs. After 8 d of culture, these peritoneal cultured MCs (PCMCs) were enriched using mouse CD117 microbeads (Miltenyi) and cultured for further 48 h to avoid MC activation. MC-deficient Mcpt5-Cre$^+$ R-DTA$^+$ mice and Mcpt5-Cre$^+$ R-DTA$^+$ × CD11c-eGFP/DTR were reconstituted by i.d. injection with 1.25 × 10^6 PCMCs from C57BL/6 WT mice into one ear and the same number of PCMCs from MHCII$^{-/-}$ mice into the contralateral ear.

DC depletion

Dermal DCs were locally depleted in ear skin of CD11c-Cre iDTR mice or Mcpt5-Cre R-DTA x CD11c-eGFP/DTR mice by i.d. injection of DT (100 ng/20 µl/ear) into the ear pinnae at 48 h after DNFB administration onto the ear skin or at 4 h and 48 h after DNFB.

Haplotype mismatch BM transfer

Genetically engineered inbred mouse strains commonly used in biomedical research differ in their inherited haploid genotype (also referred to as haplotype). 6-wk-old SJL/J recipient mice (CD45.1$^+$ MHCII haplotype H2^s) were lethally irradiated (whole body irradiation, 9 Gy; x-ray source, MaxiShot, Yxlon) before retro-orbital i.v. injection of 20 × 10^6 whole BM cells isolated from age- and sex-matched C57BL/6 donor mice (CD45.2$^+$ MHCII haplotype H2^b). After BM transplantation, mice were given neomycin-containing drinking water for 3 wk. To determine the chimerism of recipient mice, a 50-µl blood sample was isolated 2 wk after transplantation, and surface expression of CD45.1/CD45.2 on blood leukocytes was determined using flow cytometry (Fig. S3 A). An additional week later, the DC-to-MC communication was initiated in SJL/J^{B6} mice by DNFB administration, and the expression of C57BL/B6 donor cell–restricted H2^b MHCII on MCs and DCs was analyzed by flow cytometry 24 h after DNFB administration in comparison to SJL/J mice without BM transplantation. The H2^b MHCII expression analysis was performed using the specific mAb clone AF6-120.1 reported to bind to C57BL/6-restricted H2^b MHCII but to not cross-react with SJL/J H2^s MHCII. Analysis of skin DCs from C57BL/6 and SJL/J control mice with the AF6-120.1 mAb demonstrated, as expected, that C57BL/6-restricted H2^b MHCII was labeled but not SJL/J H2^s MHCII (Fig. S3 B).

Allogeneic T cell stimulation

DCs (CD45.2$^+$CD11c$^+$H2^{b+} in SJL/J^{B6}; CD45.1$^+$CD11c$^+$ in SJL/J) and MCs (CD45.1$^+$c-kit$^+$FcεRI$^+$) were sorted from same samples of ear skin cell suspension of SJL/J^{B6} chimera mice 24 h after DNFB administration and untreated SJL/J mice. Spleen DCs as positive control for allogeneic T cell stimulation were isolated from C57BL/6 mice using CD11c microbeads (Miltenyi). 2 × 10^4 DCs or MCs were seeded to 96-well cell-culture plates in 50 µl complete RPMI medium supplemented with 10% FCS and 1% penicillin/streptomycin. T cells were negatively enriched from spleens of untreated SJL/J mice using the pan T cell isolation kit (Miltenyi) and labeled with CFSE. Allogeneic T cell proliferation was verified by co-culturing 10^5 CFSE-labeled T cells with preseeded DCs or MCs over 6 d. Subsequently, CD3$^+$CD4$^+$ T cell proliferation was measured as CFSE dilution by flow cytometry and quantified as the fraction of proliferated CD4$^+$ T cells bearing low CFSE staining and as mean fluorescence intensity. Cytokines were quantified in the co-culture supernatants using the bead based mouse essential Th1/Th2 cytokine 6-plex ProcartaPlex panel (ThermoFisher).

T cell–induced skin inflammation

C57BL/6 WT donor mice were sensitized with DNFB (0.5%, 100 µl) on the shaved back, and preactivated T cells were isolated from inguinal LNs 6 d later using a pan T cell enrichment kit (Miltenyi). CD11c-Cre$^+$ iDTR mice and Cre$^-$ littermates were treated with DNFB 0.2% on the ear skin (0.2%, 20 µl/ear) followed by DC depletion at 48 h after DNFB (group 1: CD11c-Cre$^-$; and group 2: CD11c-Cre$^+$ iDTR mice) or at 4 h and 48 h after DNFB (group 3: CD11c-Cre$^+$ iDTR). Skin inflammation was induced in CD11c-Cre iDTR recipient mice by i.d. injection of 1.25 × 10^6 preactivated T cells from sensitized WT mice into the ear 72 h after recipient mice DNFB treatment and quantified by measuring the ear thickness at the indicated time points using a caliper (Mitutoyo) in relation to basal ear thickness.

Intravital 2-photon microscopy of mouse ear skin

Mice were prepared for intravital microscopy as previously described (Dudeck et al., 2011a). In brief, animals were subjected to intubation narcosis with a mixture of Isofluran (1.0%) and oxygen (99%) with a mechanical ventilator (Mini-Vent, Hugo-Sachs Elektronik). Two-photon intravital microscopy was performed with a Zeiss LSM780 NLO microscope with simultaneous detection via four external non-descanned detectors. Illumination was performed at 920 nm with a Chameleon Vision II (Coherent, Inc.) laser (10–12% laser power, at 1,400 mW maximum power) via a 20× water-dipping lens with 1.0 NA. GFP-expressing DCs were detected with a 525/50 bandpass filter (BP), tdRFP-expressing MCs with a 600/20 BP, and blood vessels by i.v. injection of 12.5 µl Qtracker 705 nontargeted Qdots (Invitrogen) in 83 µl isotonic NaCl (BP 710/40). Collagen I structures were visualized by its SHG (<485 nm, BP 450/70). For visualization, raw data were processed and reconstructed using Imaris (Bitplane) and represented as maximum intensity projection (MIP) or 3D-rendered z-stacks. Time-lapse series were recorded with a rate of 1 z-stack per minute, a pixel size of 0.24 µm, and a z-spacing of 4 µm encompassing 84 µm in z and an area of 250 × 250 µm in xy.

Image analysis

Randomly and blindly chosen image stacks were analyzed for the different experimental conditions: $n = 102$ (7 mice) before DNFB administration, $n = 30$ (5 mice) 8–12 h after DNFB, and $n = 30$ (3 mice) 24–28 h after DNFB application. For the dynamic characterization, $n = 20$ (7 mice) before DNFB, $n = 28$ (5 mice) at 8–12 h after DNFB, and $n = 23$ (3 mice) 24–28 h after DNFB time-lapse series were analyzed. Image analysis used the following channels recorded for each image stack: (a) MC signal in red and referred to as red signal, (b) DC signal in green and referred to as green signal, and (c) SHG in gray and referred to as collagen signal. The customized high-throughput image analysis included preprocessing, segmentation, and quantitative analysis steps. The preprocessing was performed in Fiji software (ImageJ version 1.49), whereas the segmentation and quantitative analysis were implemented in Python programming language (version 2.7.3). The source code (ImageJ macros and Python scripts) with exact settings of each image analysis step is available upon request. Preprocessing of images included noise suppression with a median and a Gaussian filter, and contrast enhancement by normalization to the 95th percentile. Furthermore, deconvolution of the MC and DC channel was performed to compensate for the point spread function of the microscope using the Iterative Deconvolve 3D plug-in (version 5.2.) in Fiji software (Dong et al., 2003).

The removal of autofluorescence artifacts was performed in two steps. First, each two-dimensional (2D) layer was analyzed separately (Fig. S1, A and B), in order to eliminate prominent artifacts (e.g., large areas of corneocytes) and thus reduce computational time needed for 3D labeling and analysis of objects. After that, each connected 3D region was quantitatively characterized with respect to its size, shape, and intensity of different channels and then classified as an artifact or a MC (Fig. S1 C). Selection of parameters for the artifacts removal and the threshold values for these parameters was done based on distributions of corresponding parameters in all objects (Fig. S1 D). The watershed transformation for separation of touching MCs was performed on the preprocessed red (MC) channel; the seed points were identified as local maxima in the additionally smoothed image.

Sensitivity and precision of image segmentation. The sensitivity S and precision P of the segmentation was evaluated using 15% of all static data stacks, where the number of false positives (FP) and false negatives (FN) was manually counted. The number of true positives (TP) was computed as the difference between the number of automatically detected cells and the number of FP. Sensitivity and precision of the segmentation were computed as follows for all MCs, interacting MCs, and double-positive MCs:

$$S = \frac{TP}{TP + FN},$$
$$P = \frac{TP}{TP + FP}.$$

Quantitative characterization of static data. The quantitative analysis of static data involved, first, characterization of each individual MC, and then characterization of each image stack based on the data of individual MCs. Analysis of individual MCs included characterization of their size and morphology, the distance to DCs (to register interactions), and the green signal of MCs (to detect double-positive MCs). The size D was computed from the volume formula

$$D = 2\sqrt[3]{\frac{3}{4\pi}V},$$

where V is the volume of an object in μm^3 (number of voxels multiplied by the voxel size). The shape was characterized by the eccentricity:

$$E = \frac{Q95(d)}{Q5(d)},$$

where d is an array of distances from the object's centroid to border points, and $Q5$ and $Q95$ are the 5th and 95th percentiles of d. The distance to DC was computed as the closest distance from the border of a MC to the nearest DC. A MC was considered to be interacting if this distance was equal to zero, i.e., if the masks of MC and DC were overlapping. The green signal of MCs was characterized by the median of the green-to-red signal ratio in the MC region that does not overlap with DCs. A MC was considered to be double-positive if this median was greater than 0.25. This threshold corresponds to the separating value in the bimodal distribution of the median red signal for all cells, with ordinary MCs on the one hand and double-positive MCs and artifacts on the other hand (Fig. S1 D). The analysis of image stacks involved computing the fractions of interacting and double-positive MCs, which were assessed as the number of interacting/double-positive MCs in a stack divided by the total number of MCs.

Quantitative characterization of dynamic data. To characterize the dynamics of cell interactions, tracking of MCs from one time frame to another was needed. Because of the relatively slow migration of MCs compared with the time resolution between subsequent frames, this could be performed by means of the nearest neighbor tracking approach. We used the coordinates of the cells' centroids, which were extracted during the quantitative characterization of individual MCs. The analysis of time-lapse data aimed at characterizing the dynamics of interactions under different experimental conditions. Additionally, the dynamics of MC shape were analyzed. To characterize the dynamics of cellular shape (Fig. 3 D, a shape change characteristic (dS_n) was computed for each MC track n, as the median of a shape change $dS_{n,t}$ at individual time points t: $dS_n = Md(dS_{n,t})$, $t \in [0; T_n]$, where T_n is the length of the n-th track, and $Md(\,)$ denotes the median value. The shape change at each time point t for the cell t was computed as follows:

$$dS_{n,t} = \frac{\sum_{x,y,z}(M_{n,t} \oplus M_{n,t-1})}{\sum_{x,y,z}(M_{n,t} \vee M_{n,t-1})},$$

where $\oplus$ denotes the logical "exclusive or" operation and $\vee$ denotes the logical "or" operation. The numerator of this expression corresponds to the difference between the masks $M_{n,t-1}$ and $M_{n,t}$ at subsequent time points, and the denominator corresponds to the union of these masks, where $M_{n,t}$ denotes the MC mask of track n at time t with $M_{n,t} = 1$ if the n-th MC is present and $M_{n,t} = 0$ otherwise.

Characterization of the dynamics of interactions involved computing the dynamics of overlap between MC and DC, as well as several characteristics of cell contacts (Fig. S2). To characterize the overlap dynamics, an overlap change characteristic (dO_n) was computed: the changes in the cells' overlap ($O_{n,t}$) were analyzed over time analogously to the changes in shape $M_{n,t}$ (Fig. S1 D). The characterization of cell contacts (Fig. S2 B) included computing the number of contacts (N_n) that each MC experiences during the whole time period T_n of its cell track, the mean duration of such contacts for each MC ($\bar{L}_n$), the total time that each MC stays in contact with a DC (L_n), and the ratio of the time of contact to the whole tracking period (R_n).

Statistical analysis

In imaging analysis, the statistical evaluation of differences between experimental groups was done using the Wilcoxon rank-sum test. To prevent an influence of a too large sample size on the outcome of the statistical tests in the comparison between individual MCs, a randomization scheme was implemented. This scheme involved random selection of 100 cells in each of the experimental groups, testing them with the Wilcoxon rank-sum test, and repeating the procedure 10 times such that no cell is analyzed more than once. The P values of the 10 rounds of tests were combined using Fisher's method (Fisher, 1925). For statistical comparison of stack characteristics, an analogous procedure was performed to compensate for unequal sample sizes of the different experimental conditions (102, 30, and 30 stacks were analyzed in each of the three experimental conditions, respectively). Here, three subsets, 30 stacks each, were randomly selected from the first group, and three independent statistical tests were performed. In the second and the third groups, all 30 stacks were analyzed each time. The p-values of three rounds of tests were again combined using Fisher's method (Fisher, 1925).

For non-imaging analysis, the statistical evaluation of differences between experimental groups was done using Student's t test. P-values are designated as follows: *, $P < 0.05$; **, $P < 0.01$; and ***, $P < 0.001$, except as otherwise noted in the figure legends.

Online supplemental material

Fig. S1 shows the decision workflow for artifacts removal. Fig. S2 shows dynamic analysis of DC-to-MC interactions over time. Fig. S3 shows analysis of CD45.2 and H-2^b MHCII expression by SJL/J^{B6} BM chimera DCs. Fig. S4 shows sorting of skin DCs and MCs from SJL/J^{B6} BM mice. Video 1 shows DC migrational arrest upon DNFB administration. Video 2 shows time-lapse series in DC^{GFP}/MC^{RFP} mouse ear skin before DNFB treatment. Video 3 shows time-lapse series in DC^{GFP}/MC^{RFP} mouse ear skin 12 h after DNFB treatment. Video 4 shows time-lapse series in DC^{GFP}/MC^{RFP} mouse ear skin 24 h after DNFB treatment. Video 5 shows DC/MC single-pair time-lapse series in DC^{GFP}/MC^{RFP} mouse ear skin before DNFB treatment. Video 6 shows close-up time-lapse series in DC^{GFP}/MC^{RFP} mouse ear skin before DNFB treatment. Video 7 shows DC/MC single-pair time-lapse series in DC^{GFP}/MC^{RFP} mouse ear skin 8 h after DNFB treatment. Video 8 shows close-up time-lapse series of DC^{GFP}/MC^{RFP} mouse ear skin 8 h after DNFB treatment. Video 9 shows DC/MC single-pair time-lapse series in DC^{GFP}/MC^{RFP} mouse ear skin 14 h after DNFB treatment. Video 10 shows close-up time-lapse series of DC^{GFP}/MC^{RFP} mouse ear skin 14 h after DNFB treatment. Video 11 shows DC/MC single-pair time-lapse series in DC^{GFP}/MC^{RFP} mouse ear skin 24 h after DNFB treatment. Video 12 shows close-up time-lapse series of DC^{GFP}/MC^{RFP} mouse ear skin 24 h after DNFB treatment. Video 13 shows single z-plane time-lapse series of a GFP^+RFP^+MC in contact with DCs in DC^{GFP}/MC^{RFP} mouse ear skin 24 h after DNFB treatment, showing the intercellular transfer of GFP^+ vesicles.

ACKNOWLEDGMENTS

We cordially thank A. Roers for providing the *Mcpt5-Cre* mouse line, H.J. Fehling for providing the tdRFP line, A. Waisman for iDTR, and D. Voehringer for R-DTA mice. Expert technical assistance by C. Haase, T. Häring, C. Kühn, A. Gröbe, K. Hüttner, and A. Karutz is gratefully acknowledged. We further thank the Core Facility Imaging, Medical Faculty Carl Gustav Carus, Technische Universität Dresden, for advice and provision of processing capacities.

This work was supported by grants from the German Research Foundation (DFG; grants DU1172/2 [Priority Program 1468] and DU1172/3 [Priority Program 1394]) to A. Dudeck.

The authors declare no competing financial interests.

Author contributions: J. Dudeck, A. Medyukhina, M.T. Figge, and A. Dudeck designed and conducted the study and wrote the manuscript. J. Dudeck, A. Medyukhina, A. Dudeck, M.T. Figge, J. Fröbel, C.-M. Svensson, J. Kotrba, M. Gerlach, and A.-C. Gradtke performed experiments and analyzed data. J. Dudeck, A. Medyukhina, A. Dudeck, M.T. Figge, B. Schröder, and S. Speier interpreted data. All authors approved the final version of the manuscript.

Submitted: 27 May 2016

Revised: 14 July 2017

Accepted: 13 September 2017

REFERENCES

Abraham, S.N., and A.L. St. John. 2010. Mast cell-orchestrated immunity to pathogens. *Nat. Rev. Immunol.* 10:440–452. https://doi.org/10.1038/nri2782

Blank, U., F.H. Falcone, and G. Nilsson. 2013. The history of mast cell and basophil research - some lessons learnt from the last century. *Allergy.* 68:1093–1101. https://doi.org/10.1111/all.12197

Bour, H., E. Peyron, M. Gaucherand, J.L. Garrigue, C. Desvignes, D. Kaiserlian, J.P. Revillard, and J.F. Nicolas. 1995. Major histocompatibility complex class I-restricted CD8+ T cells and class II-restricted CD4+ T cells, respectively, mediate and regulate contact sensitivity to dinitrofluorobenzene. *Eur. J. Immunol.* 25:3006–3010. https://doi.org/10.1002/eji.1830251103

Buch, T., F.L. Heppner, C. Tertilt, T.J. Heinen, M. Kremer, F.T. Wunderlich, S. Jung, and A. Waisman. 2005. A Cre-inducible diphtheria toxin receptor mediates cell lineage ablation after toxin administration. *Nat. Methods.* 2:419–426. https://doi.org/10.1038/nmeth762

Campana, S., C. De Pasquale, P. Carrega, G. Ferlazzo, and I. Bonaccorsi. 2015. Cross-dressing: an alternative mechanism for antigen presentation. *Immunol. Lett.* 168:349–354. https://doi.org/10.1016/j.imlet.2015.11.002

Carroll-Portillo, A., Z. Surviladze, A. Cambi, D.S. Lidke, and B.S. Wilson. 2012. Mast cell synapses and exosomes: membrane contacts for information exchange. *Front. Immunol.* 3:46. https://doi.org/10.3389/fimmu.2012.00046

Carroll-Portillo, A., J.L. Cannon, J. te Riet, A. Holmes, Y. Kawakami, T. Kawakami, A. Cambi, and D.S. Lidke. 2015. Mast cells and dendritic cells form synapses that facilitate antigen transfer for T cell activation. *J. Cell Biol.* 210:851–864. https://doi.org/10.1083/jcb.201412074

Coelho, F.M., D. Natale, S.F. Soriano, M. Hons, J. Swoger, J. Mayer, R. Danuser, E. Scandella, M. Pieczyk, H.-G. Zerwes, et al. 2013. Naive B-cell trafficking is shaped by local chemokine availability and LFA-1-independent stromal interactions. *Blood.* 121:4101–4109. https://doi.org/10.1182/blood-2012-10-465336

De Filippo, K., A. Dudeck, M. Hasenberg, E. Nye, N. van Rooijen, K. Hartmann, M. Gunzer, A. Roers, and N. Hogg. 2013. Mast cell and macrophage chemokines CXCL1/CXCL2 control the early stage of neutrophil recruitment during tissue inflammation. *Blood.* 121:4930–4937. https://doi.org/10.1182/blood-2013-02-486217

Dolan, B.P., K.D. Gibbs Jr., and S. Ostrand-Rosenberg. 2006a. Tumor-specific CD4+ T cells are activated by "cross-dressed" dendritic cells presenting peptide-MHC class II complexes acquired from cell-based cancer vaccines. *J. Immunol.* 176:1447–1455. https://doi.org/10.4049/jimmunol.176.3.1447

Dolan, B.P., K.D. Gibbs Jr., and S. Ostrand-Rosenberg. 2006b. Dendritic cells cross-dressed with peptide MHC class I complexes prime CD8+ T cells. *J. Immunol.* 177:6018–6024. https://doi.org/10.4049/jimmunol.177.9.6018

Dong, C.-Y., K. Koenig, and P. So. 2003. Characterizing point spread functions of two-photon fluorescence microscopy in turbid medium. *J. Biomed. Opt.* 8:450–459. https://doi.org/10.1117/1.1578644

Dudeck, A., J. Dudeck, J. Scholten, A. Petzold, S. Surianarayanan, A. Köhler, K. Peschke, D. Vöhringer, C. Waskow, T. Krieg, et al. 2011a. Mast cells are key promoters of contact allergy that mediate the adjuvant effects of haptens. *Immunity.* 34:973–984. https://doi.org/10.1016/j.immuni.2011.03.028

Dudeck, A., C.A. Suender, S.L. Kostka, E. von Stebut, and M. Maurer. 2011b. Mast cells promote Th1 and Th17 responses by modulating dendritic cell maturation and function. *Eur. J. Immunol.* 41:1883–1893. https://doi.org/10.1002/eji.201040994

Dudeck, J., S.M. Ghouse, C.H.K. Lehmann, A. Hoppe, N. Schubert, S.A. Nedospasov, D. Dudziak, and A. Dudeck. 2015. Mast-Cell-Derived TNF Amplifies CD8(+) Dendritic Cell Functionality and CD8(+) T Cell Priming. *Cell Reports.* 13:399–411. https://doi.org/10.1016/j.celrep.2015.08.078

Figge, M.T., and M. Meyer-Hermann. 2011. Modelling intravital two-photon data of lymphocyte migration and interaction. *In* Mathematical Models and Immune Cell Biology. C. Molina-París, and G. Lythe, editors. Springer, Heidelberg. pp. 121–139. https://doi.org/10.1007/978-1-4419-7725-0_6

Figge, M.T., A. Garin, M. Gunzer, M. Kosco-Vilbois, K.-M. Toellner, and M. Meyer-Hermann. 2008. Deriving a germinal center lymphocyte migration model from two-photon data. *J. Exp. Med.* 205:3019–3029. https://doi.org/10.1084/jem.20081160

Fisher, R.A. 1925. Statistical methods for research workers. Genesis Publishing Pvt Ltd.

Fyhrquist, N., H. Wolff, A. Lauerma, and H. Alenius. 2012. CD8+ T cell migration to the skin requires CD4+ help in a murine model of contact hypersensitivity. *PLoS One.* 7:e41038. https://doi.org/10.1371/journal.pone.0041038

Galli, S.J., and M. Tsai. 2012. IgE and mast cells in allergic disease. *Nat. Med.* 18:693–704. https://doi.org/10.1038/nm.2755

Galli, S.J., S. Nakae, and M. Tsai. 2005. Mast cells in the development of adaptive immune responses. *Nat. Immunol.* 6:135–142. https://doi.org/10.1038/ni1158

Garin, A., M. Meyer-Hermann, M. Contie, M.T. Figge, V. Buatois, M. Gunzer, K.-M. Toellner, G. Elson, and M.H. Kosco-Vilbois. 2010. Toll-like receptor 4 signaling by follicular dendritic cells is pivotal for germinal center onset and affinity maturation. *Immunity.* 33:84–95. https://doi.org/10.1016/j.immuni.2010.07.005

Gaudenzio, N., N. Espagnolle, L.T. Mars, R. Liblau, S. Valitutti, and E. Espinosa. 2009. Cell-cell cooperation at the T helper cell/mast cell immunological synapse. *Blood.* 114:4979–4988. https://doi.org/10.1182/blood-2009-02-202648

Gaudenzio, N., C. Laurent, S. Valitutti, and E. Espinosa. 2013. Human mast cells drive memory CD4+ T cells toward an inflammatory IL-22+ phenotype. *J. Allergy Clin. Immunol.* 131:1400–7.e11. https://doi.org/10.1016/j.jaci.2013.01.029

Gerdes, H.H., and R.N. Carvalho. 2008. Intercellular transfer mediated by tunneling nanotubes. *Curr. Opin. Cell Biol.* 20:470–475. https://doi.org/10.1016/j.ceb.2008.03.005

Gocinski, B.L., and R.E. Tigelaar. 1990. Roles of CD4+ and CD8+ T cells in murine contact sensitivity revealed by in vivo monoclonal antibody depletion. *J. Immunol.* 144:4121–4128.

Gorbachev, A.V., P.S. Heeger, and R.L. Fairchild. 2001. CD4+ and CD8+ T cell priming for contact hypersensitivity occurs independently of CD40-CD154 interactions. *J. Immunol.* 166:2323–2332. https://doi.org/10.4049/jimmunol.166.4.2323

He, D., L. Wu, H.K. Kim, H. Li, C.A. Elmets, and H. Xu. 2006. CD8+ IL-17-producing T cells are important in effector functions for the elicitation of contact hypersensitivity responses. *J. Immunol.* 177:6852–6858. https://doi.org/10.4049/jimmunol.177.10.6852

Huang, J.F., Y. Yang, H. Sepulveda, W. Shi, I. Hwang, P.A. Peterson, M.R. Jackson, J. Sprent, and Z. Cai. 1999. TCR-Mediated internalization of peptide-MHC complexes acquired by T cells. *Science.* 286:952–954. https://doi.org/10.1126/science.286.5441.952

Hudrisier, D., J. Riond, H. Mazarguil, J.E. Gairin, and E. Joly. 2001. Cutting edge: CTLs rapidly capture membrane fragments from target cells in a TCR signaling-dependent manner. *J. Immunol.* 166:3645–3649. https://doi.org/10.4049/jimmunol.166.6.3645

Hudson, L., and J. Sprent. 1976. Specific adsorption of IgM antibody onto H-2-activated mouse T lymphocytes. *J. Exp. Med.* 143:444–449. https://doi.org/10.1084/jem.143.2.444

Hudson, L., J. Sprent, J.F. Miller, and J.H. Playfair. 1974. B cell-derived immunoglobulin on activated mouse T lymphocytes. *Nature.* 251:60–62. https://doi.org/10.1038/251060a0

Jawdat, D.M., G. Rowden, and J.S. Marshall. 2006. Mast cells have a pivotal role in TNF-independent lymph node hypertrophy and the mobilization of Langerhans cells in response to bacterial peptidoglycan. *J. Immunol.* 177:1755–1762. https://doi.org/10.4049/jimmunol.177.3.1755

Joly, E., and D. Hudrisier. 2003. What is trogocytosis and what is its purpose? *Nat. Immunol.* 4:815. https://doi.org/10.1038/ni0903-815

Joulia, R., N. Gaudenzio, M. Rodrigues, J. Lopez, N. Blanchard, S. Valitutti, and E. Espinosa. 2015. Mast cells form antibody-dependent degranulatory synapse for dedicated secretion and defence. *Nat. Commun.* 6:6174. https://doi.org/10.1038/ncomms7174

Jung, S., D. Unutmaz, P. Wong, G. Sano, K. De los Santos, T. Sparwasser, S. Wu, S. Vuthoori, K. Ko, F. Zavala, et al. 2002. In vivo depletion of CD11c+ dendritic cells abrogates priming of CD8+ T cells by exogenous cell-associated antigens. *Immunity.* 17:211–220. https://doi.org/10.1016/S1074-7613(02)00365-5

Kambayashi, T., E.J. Allenspach, J.T. Chang, T. Zou, J.E. Shoag, S.L. Reiner, A.J. Caton, and G.A. Koretzky. 2009. Inducible MHC class II expression by mast cells supports effector and regulatory T cell activation. *J. Immunol.* 182:4686–4695. https://doi.org/10.4049/jimmunol.0803180

Kaplan, D.H., B.Z. Igyártó, and A.A. Gaspari. 2012. Early immune events in the induction of allergic contact dermatitis. *Nat. Rev. Immunol.* 12:114–124. https://doi.org/10.1038/nri3150

Kehren, J., C. Desvignes, M. Krasteva, M.T. Ducluzeau, O. Assossou, F. Horand, M. Hahne, D. Kägi, D. Kaiserlian, and J.F. Nicolas. 1999. Cytotoxicity is mandatory for CD8(+) T cell-mediated contact hypersensitivity. *J. Exp. Med.* 189:779–786. https://doi.org/10.1084/jem.189.5.779

Kish, D.D., X. Li, and R.L. Fairchild. 2009. CD8 T cells producing IL-17 and IFN-gamma initiate the innate immune response required for responses to antigen skin challenge. *J. Immunol.* 182:5949–5959. https://doi.org/10.4049/jimmunol.0802830

Kitawaki, T., N. Kadowaki, N. Sugimoto, N. Kambe, T. Hori, Y. Miyachi, T. Nakahata, and T. Uchiyama. 2006. IgE-activated mast cells in combination with pro-inflammatory factors induce Th2-promoting dendritic cells. *Int. Immunol.* 18:1789–1799. https://doi.org/10.1093/intimm/dxl113

Lanzavecchia, A., and F. Sallusto. 2001. Regulation of T cell immunity by dendritic cells. *Cell.* 106:263–266. https://doi.org/10.1016/S0092-8674(01)00455-X

Lazarski, C.A., F.A. Chaves, S.A. Jenks, S. Wu, K.A. Richards, J.M. Weaver, and A.J. Sant. 2005. The kinetic stability of MHC class II:peptide complexes is a key parameter that dictates immunodominance. *Immunity.* 23:29–40. https://doi.org/10.1016/j.immuni.2005.05.009

Ley, K. 2014. The second touch hypothesis: T cell activation, homing and polarization. *F1000 Res.* 3:37. https://doi.org/10.12688/f1000research.3-37.v2

Liu, J., E. Harberts, A. Tammaro, N. Girardi, R.B. Filler, R. Fishelevich, A. Temann, P. Licona-Limón, M. Girardi, R.A. Flavell, and A.A. Gaspari. 2014. IL-9 regulates allergen-specific Th1 responses in allergic contact dermatitis. *J. Invest. Dermatol.* 134:1903–1911. https://doi.org/10.1038/jid.2014.61

Luche, H., O. Weber, T. Nageswara Rao, C. Blum, and H.J. Fehling. 2007. Faithful activation of an extra-bright red fluorescent protein in "knock-in" Cre-reporter mice ideally suited for lineage tracing studies. *Eur. J. Immunol.* 37:43–53. https://doi.org/10.1002/eji.200636745

Lyon, M.F., and A.G. Searle. 1989. Genetic Variants and Strains of the Laboratory Mouse. Second edition. Oxford University Press, New York.

Madsen, L., N. Labrecque, J. Engberg, A. Dierich, A. Svejgaard, C. Benoist, D. Mathis, and L. Fugger. 1999. Mice lacking all conventional MHC class II genes. *Proc. Natl. Acad. Sci. USA.* 96:10338–10343. https://doi.org/10.1073/pnas.96.18.10338

Martin, S.F. 2012. Allergic contact dermatitis: xenoinflammation of the skin. *Curr. Opin. Immunol.* 24:720–729. https://doi.org/10.1016/j.coi.2012.08.003

Martin, S.F. 2015. Immunological mechanisms in allergic contact dermatitis. *Curr. Opin. Allergy Clin. Immunol.* 15:124–130. https://doi.org/10.1097/ACI.0000000000000142

Medyukhina, A., S. Timme, Z. Mokhtari, and M.T. Figge. 2015. Image-based systems biology of infection. *Cytometry A.* 87:462–470. https://doi.org/10.1002/cyto.a.22638

Meyer-Hermann, M., M.T. Figge, and K.-M. Toellner. 2009. Germinal centres seen through the mathematical eye: B-cell models on the catwalk. *Trends Immunol.* 30:157–164. https://doi.org/10.1016/j.it.2009.01.005

Mokhtari, Z., F. Mech, C. Zitzmann, M. Hasenberg, M. Gunzer, and M.T. Figge. 2013. Automated characterization and parameter-free classification of cell tracks based on local migration behavior. *PLoS One.* 8:e80808. (published erratum appears in *PLoS One*. 2014. 9:e115158) https://doi.org/10.1371/journal.pone.0080808

Otsuka, A., M. Kubo, T. Honda, G. Egawa, S. Nakajima, H. Tanizaki, B. Kim, S. Matsuoka, T. Watanabe, S. Nakae, et al. 2011. Requirement of interaction between mast cells and skin dendritic cells to establish contact hypersensitivity. *PLoS One.* 6:e25538. https://doi.org/10.1371/journal.pone.0025538

Peiser, M. 2013. Role of Th17 cells in skin inflammation of allergic contact dermatitis. *Clin. Dev. Immunol.* 2013:261037. https://doi.org/10.1155/2013/261037

Peschke, K., A. Weitzmann, K. Heger, R. Behrendt, N. Schubert, J. Scholten, D. Voehringer, K. Hartmann, A. Dudeck, M. Schmidt-Supprian, and A. Roers. 2014. IκB kinase 2 is essential for IgE-induced mast cell de novo cytokine production but not for degranulation. *Cell Reports.* 8:1300–1307. https://doi.org/10.1016/j.celrep.2014.07.046

Peschke, K., A. Dudeck, A. Rabenhorst, K. Hartmann, and A. Roers. 2015. Cre/loxP-based mouse models of mast cell deficiency and mast cell-specific gene inactivation. *Methods Mol. Biol.* 1220:403–421. https://doi.org/10.1007/978-1-4939-1568-2_25

Reber, L.L., R. Sibilano, P. Starkl, A. Roers, M.A. Grimbaldeston, M. Tsai, N. Gaudenzio, and S.J. Galli. 2017. Imaging protective mast cells in living mice during severe contact hypersensitivity. *JCI Insight.* 2:92900; Epub ahead of print. https://doi.org/10.1172/jci.insight.92900

Scholten, J, K Hartmann, A Gerbaulet, T Krieg, W Müller, G Testa, and A Roers. 2008. Mast cell-specific Cre/loxP-mediated recombination in vivo. *Transgenic Research.* 17:307–315. https://doi.org/10.1007/s11248-007-9153-4

Schubert, N., J. Dudeck, P. Liu, A. Karutz, S. Speier, M. Maurer, J. Tuckermann, and A. Dudeck. 2015. Mast cell promotion of T cell-driven antigen-induced arthritis despite being dispensable for antibody-induced arthritis in which T cells are bypassed. *Arthritis Rheumatol.* 67:903–913. https://doi.org/10.1002/art.38996

Sharrow, S.O., B.J. Mathieson, and A. Singer. 1981. Cell surface appearance of unexpected host MHC determinants on thymocytes from radiation bone marrow chimeras. *J. Immunol.* 126:1327–1335.

Shelburne, C.P., H. Nakano, A.L. St. John, C. Chan, J.B. McLachlan, M.D. Gunn, H.F. Staats, and S.N. Abraham. 2009. Mast cells augment adaptive immunity by orchestrating dendritic cell trafficking through infected tissues. *Cell Host Microbe.* 6:331–342. https://doi.org/10.1016/j.chom.2009.09.004

Simon, D., C. Aeberhard, Y. Erdemoglu, and H.U. Simon. 2014. Th17 cells and tissue remodeling in atopic and contact dermatitis. *Allergy.* 69:125–131. https://doi.org/10.1111/all.12351

Stinchcombe, J.C., G. Bossi, S. Booth, and G.M. Griffiths. 2001. The immunological synapse of CTL contains a secretory domain and membrane bridges. *Immunity.* 15:751–761. https://doi.org/10.1016/S1074-7613(01)00234-5

St. John, A.L., and S.N. Abraham. 2013. Innate immunity and its regulation by mast cells. *J. Immunol.* 190:4458–4463. https://doi.org/10.4049/jimmunol.1203420

Suto, H., S. Nakae, M. Kakurai, J.D. Sedgwick, M. Tsai, and S.J. Galli. 2006. Mast cell-associated TNF promotes dendritic cell migration. *J. Immunol.* 176:4102–4112. https://doi.org/10.4049/jimmunol.176.7.4102

Valitutti, S., R. Joulia, and E. Espinosa. 2017. The Mast Cell Antibody-Dependent Degranulatory Synapse. *Methods Mol. Biol.* 1584:487–495. https://doi.org/10.1007/978-1-4939-6881-7_30

Voehringer, D., H.E. Liang, and R.M. Locksley. 2008. Homeostasis and effector function of lymphopenia-induced "memory-like" T cells in constitutively T cell-depleted mice. *J. Immunol.* 180:4742–4753. https://doi.org/10.4049/jimmunol.180.7.4742

Watkins, S.C., and R.D. Salter. 2005. Functional connectivity between immune cells mediated by tunneling nanotubules. *Immunity.* 23:309–318. https://doi.org/10.1016/j.immuni.2005.08.009

Weber, F.C., T. Németh, J.Z. Csepregi, A. Dudeck, A. Roers, B. Ozsvári, E. Oswald, L.G. Puskás, T. Jakob, A. Mócsai, and S.F. Martin. 2015. Neutrophils are required for both the sensitization and elicitation phase of contact hypersensitivity. *J. Exp. Med.* 212:15–22. https://doi.org/10.1084/jem.20130062

Zhang, Y., M. Meyer-Hermann, L.A. George, M.T. Figge, M. Khan, M. Goodall, S.P. Young, A. Reynolds, F. Falciani, A. Waisman, et al. 2013. Germinal center B cells govern their own fate via antibody feedback. *J. Exp. Med.* 210:457–464. https://doi.org/10.1084/jem.20120150

Zhao, Y., A. Balato, R. Fishelevich, A. Chapoval, D.L. Mann, and A.A. Gaspari. 2009. Th17/Tc17 infiltration and associated cytokine gene expression in elicitation phase of allergic contact dermatitis. *Br. J. Dermatol.* 161:1301–1306. https://doi.org/10.1111/j.1365-2133.2009.09400.x